

1-1-2006

## Shielding and radiation dose analysis for a dense-plasma focus neutron source

Robert James O'Brien  
*University of Nevada, Las Vegas*

Follow this and additional works at: <https://digitalscholarship.unlv.edu/rtds>

---

### Repository Citation

O'Brien, Robert James, "Shielding and radiation dose analysis for a dense-plasma focus neutron source" (2006). *UNLV Retrospective Theses & Dissertations*. 2026.  
<http://dx.doi.org/10.25669/xno8-wxu2>

This Thesis is protected by copyright and/or related rights. It has been brought to you by Digital Scholarship@UNLV with permission from the rights-holder(s). You are free to use this Thesis in any way that is permitted by the copyright and related rights legislation that applies to your use. For other uses you need to obtain permission from the rights-holder(s) directly, unless additional rights are indicated by a Creative Commons license in the record and/or on the work itself.

This Thesis has been accepted for inclusion in UNLV Retrospective Theses & Dissertations by an authorized administrator of Digital Scholarship@UNLV. For more information, please contact [digitalscholarship@unlv.edu](mailto:digitalscholarship@unlv.edu).

**SHIELDING AND RADIATION DOSE ANALYSIS FOR A DENSE-PLASMA  
FOCUS NEUTRON SOURCE**

by

**Robert James O'Brien**

**Bachelor of Science, Mechanical Engineering  
University of Nevada, Las Vegas  
2005**

**Bachelor of Science, Applied Physics  
University of Nevada, Las Vegas  
2005**

**A thesis submitted in partial fulfillment  
of the requirements for the**

**Master of Science Degree in Materials and Nuclear Engineering  
Department of Mechanical Engineering  
Howard R. Hughes College of Engineering**

**Graduate College  
University of Nevada, Las Vegas  
August 2006**

UMI Number: 1439977

### INFORMATION TO USERS

The quality of this reproduction is dependent upon the quality of the copy submitted. Broken or indistinct print, colored or poor quality illustrations and photographs, print bleed-through, substandard margins, and improper alignment can adversely affect reproduction.

In the unlikely event that the author did not send a complete manuscript and there are missing pages, these will be noted. Also, if unauthorized copyright material had to be removed, a note will indicate the deletion.

**UMI**<sup>®</sup>

---

UMI Microform 1439977

Copyright 2007 by ProQuest Information and Learning Company.

All rights reserved. This microform edition is protected against unauthorized copying under Title 17, United States Code.

ProQuest Information and Learning Company  
300 North Zeeb Road  
P.O. Box 1346  
Ann Arbor, MI 48106-1346



**Thesis Approval**  
The Graduate College  
University of Nevada, Las Vegas

July 20 \_\_\_\_\_, 20<sup>06</sup>

The Thesis prepared by  
Robert J. O'Brien

**Entitled**

Shielding and Radiation Dose Analysis for a Dense-Plasma Focus  
Neutron Source

is approved in partial fulfillment of the requirements for the degree of  
Master of Science in Materials and Nuclear Engineering

Examination Committee Chair

Dean of the Graduate College

Examination Committee Member

Examination Committee Member

Graduate College Faculty Representative

## ABSTRACT

### **Shielding and Radiation Dose Analysis for a Dense-Plasma Focus Neutron Source**

by

Robert James O'Brien

Dr. William Culbreth, Examination Committee Chair  
Professor of Engineering  
University of Nevada, Las Vegas

A dense-plasma focus device or DPF creates a very dense focus point of plasma with temperatures high enough to induce fusion reactions. One such device currently located in Las Vegas is scheduled for relocation to the Nevada Test Site. At the Test Site the device will be fired with deuterium and tritium (D-T) fusion resulting in a yield of about  $10^{13}$  fusion neutrons of 14 MeV. This poses a radiological hazard to scientists and personnel operating the device. The goal of this project was to evaluate various shielding options under consideration for the DPF operating with D-T fusion. Shields of varying neutron-shielding effectiveness were investigated using concrete, dirt, polyethylene, paraffin and borated materials. The most effective shield, a labyrinth structure, allowed almost 2000 shots per year while keeping personnel under 100 mrem of dose. The most cost effective shield that used an existing pit allowed about 350 shots per year.

## TABLE OF CONTENTS

ABSTRACT .....	iii
LIST OF TABLES.....	v
LIST OF FIGURES .....	vi
ACKNOWLEDGMENTS .....	viii
CHAPTER 1 INTRODUCTION.....	1
CHAPTER 2 REVIEW OF RELATED LITERATURE .....	4
CHAPTER 3 THEORY.....	7
3.1 The Fundamentals of Radiation.....	7
3.2 Theory of Health Physics .....	12
3.3 How the Dense-Plasma Focus Device Functions.....	16
3.4 Theory of Radiation Shielding .....	21
3.5 Theory of MCNPX.....	28
CHAPTER 4 METHODOLOGY.....	32
4.1 The DPF Device as a Radiation Source .....	32
4.2 Shielding Configurations.....	33
CHAPTER 5 RESULTS.....	38
5.1 Comparison of Dose Calculation Methods.....	38
5.2 Square Shield Results .....	48
5.3 Labyrinth Results.....	56
5.4 Cave Shield Results.....	62
CHAPTER 6 CONCLUSIONS.....	71
APPENDIX I SAMPLE MCNPX INPUT DECK .....	73
APPENDIX II SAMPLE MCNPX OUTPUT DECK .....	78
BIBLIOGRAPHY .....	86
VITA.....	88

## LIST OF TABLES

Table 3.1	Quality Factors for Radiations from NRC Regulation 10CFR20 .....	12
Table 3.2	Quality Factors for Neutrons of Known Energies .....	13
Table 3.3	Hand Calculation and MCNPX calculation of Flux in Figure 3.7 .....	27
Table 5.1	Neutron Flux-to-Dose Conversion Factors from NRC Regulations .....	39
Table 5.2	Dose Calculation in Phantom for Energy Deposition in MCNPX .....	41
Table 5.3	Dose Contribution in Tissue from Radiation Types .....	44
Table 5.4	Dose at Tally Location in Figure 13 Using Two Different Methods .....	46
Table 5.5	Comparison of Flux Calculated by MCNPX and $1/r^2$ .....	48
Table 5.6	Composition of "Portland" Concrete used in this Study with density of 2.3 g/cm <sup>3</sup> .....	51
Table 5.7	Doses at Six Tally Locations for Square Shield with Top from a $10^{13}$ Yield of 14 MeV Neutrons .....	51
Table 5.8	Doses For Square Shield with Additional Materials from a $10^{13}$ Yield of 14 MeV Neutrons .....	53
Table 5.9	Neutron Doses for Square Shield with Additional Inner Shielding from a $10^{13}$ Yield of 14 MeV Neutrons .....	55
Table 5.10	Neutron Doses for Labyrinth Shield from a $10^{13}$ Yield of 14 MeV Neutrons .....	58
Table 5.11	Neutron Doses for Labyrinth Shield with Non-Borated Materials from a $10^{13}$ Yield of 14 MeV Neutrons .....	59
Table 5.12	Neutron Doses with Thinner 18in Concrete Walls from a $10^{13}$ Yield of 14 MeV Neutrons .....	61
Table 5.13	Neutron Doses with Cave Shield from a $10^{13}$ Yield of 14 MeV Neutrons ..	63
Table 5.14	Neutron Doses with Cave Shield and no Roof from a $10^{13}$ Yield of 14 MeV Neutrons.....	64
Table 5.15	Neutron Doses with Pit Shield from a $10^{13}$ Yield of 14 MeV Neutrons .....	66
Table 5.16	Neutron Doses for Pit Shield with Polyethylene Gap Sealers from a $10^{13}$ Yield of 14 MeV Neutrons .....	68
Table 5.17	Neutron Doses for Pit Shield with Water Filled Steel Boxes as Gap Sealers from a $10^{13}$ Yield of 14 MeV Neutrons .....	69
Table 5.18	Doses to Tally Point 4 from Gammas and Neutrons for the Pit Shield Shown in fig. 5.23.....	70
Table 6.1	Summary of Dose to Tally Point 4 from all Shield Configurations .....	71

## LIST OF FIGURES

Figure 3.1	Schematic Drawing of DPF Assembly and Plasma Progression.....	17
Figure 3.2	DPF Anode, Cathode and Vacuum Chamber Assemblies .....	18
Figure 3.3	DPF Assembly and Capacitor Bank at Current Location .....	19
Figure 3.4	Neutron and Uranium Spectrum from D-D Reaction .....	20
Figure 3.5	B-10 (top) and Li-6 (bottom) Neutron Capture Cross-Sections (MCNPX)23	
Figure 3.6	Photon Cross-Sections for Lead (MCNPX).....	25
Figure 3.7	Gamma Beam Attenuation Example.....	26
Figure 3.8	225 Processor Beowulf Cluster at UNLV .....	29
Figure 3.9	Example of MCNPX Transport of Radiation Through Materials.....	30
Figure 4.1	Simple Square Shield Concept for Radiation Attenuation.....	34
Figure 4.2	“Labyrinth” Shield Configuration and Possible Escape of Radiation .....	35
Figure 4.3	“Cave” Design with Direct LOS and Potential Scattered Radiation Hazard .....	35
Figure 4.4	Existing Concrete Lined Pit Shield Concept.....	36
Figure 5.1	Cross-Sectional Views of Neutron Tracks through Phantom (MCNPX) ...	40
Figure 5.2	Comparison of MCNPX Energy Deposition Method to Flux-to-Dose Conversion.....	42
Figure 5.3	Proton Production Cross-Sections in Barns by Neutron Capture for N-14, C-12 and O-16. Hydrogen (H-1) Elastic Scattering Provided for Reference .....	44
Figure 5.4	Source and Tally Locations for Dose Method Comparison (MCNPX).....	45
Figure 5.5	Neutron Flux Spectrum at Tally Point per Source Particle.....	46
Figure 5.6	Tally Locations for Square Shield Designs.....	49
Figure 5.7	MCNPX Image of Square Shield with Top .....	50
Figure 5.8	Duct System Showing Materials (left) and Mesh Tally of Neutron Flux (right).....	50
Figure 5.9	Square Shield with Additional Shielding Materials.....	53
Figure 5.10	Total Neutron Cross Section for Polyethylene (non-borated) and Concrete .....	54
Figure 5.11	Square Shield With Additional Inner Shielding.....	55
Figure 5.12	Tally Point Locations for Labyrinth Designs.....	56
Figure 5.13	Top view of the “Labyrinth” Design.....	57
Figure 5.14	Cross-Sectional Side View of Labyrinth in Figure 23 .....	57
Figure 5.15	Mesh Tally of Neutron Tracks for the Labyrinth Concept .....	58
Figure 5.16	Labyrinth Shield with 18in Concrete Shielding.....	60
Figure 5.17	Cross-Sectional View of 18in Concrete Labyrinth Shielding.....	61
Figure 5.18	Tally Locations for “Cave” Shield.....	62
Figure 5.19	Top View of “Cave” Shield Showing Open Side .....	63

Figure 5.20	Tally Locations for Pit Shield Configuration.....	65
Figure 5.21	Side View of Pit Shield with Concrete and Poly Top.....	66
Figure 5.22	Pit Shield with Additional Polyethylene as a Gap Sealers.....	67
Figure 5.23	Pit Shield with Water Filled Steel Boxes as Gap Sealers .....	68

## ACKNOWLEDGMENTS

I would like to thank my advisor Dr. William Culbreth for his support during both this project and my graduate studies. I would also like to thank Dr. Chris Hagen for allowing me to participate in the design process for the shielding of their dense-plasma focus device.

## CHAPTER 1

### INTRODUCTION

A dense-plasma focus (DPF) device is designed to produce intense bursts of fusion neutrons in a very short-lived plasma pinch of a few nanoseconds in length. The plasma is produced by acceleration of electrons to high voltage inside a gas using large capacitor banks. Currently, Bechtel-Nevada operates a DPF device in Las Vegas using a deuterium reaction. This process uses deuterium gas in the DPF to create a fusion reaction between deuterium and deuterium (D-D) resulting in the production of approximately  $10^{11}$  neutrons of 2.45 MeV. The device is scheduled for relocation to the Nevada Test Site (NTS) where a deuterium and tritium reaction (D-T) will be demonstrated. The D-T reaction is capable of producing more energetic 14 MeV neutrons and a higher yield of  $10^{13}$  neutrons. While the intense neutron and gamma burst is useful for experimental work, there is also a large radiological hazard to workers and scientists near the machine.

Located in Las Vegas, operation of the current configuration is limited by having no shielding around the device. In order to operate, or "shoot" the device, the building must be cleared of any workers and then scientists must operate the device and experiments from outside the building. This severely limits operation since the building is multi-use and not dedicated for operation of the DPF device, resulting in less frequent shots than desired. Additionally, no shielding is provided for the scientists operating near the building in a

trailer. Utilizing a D-T reaction will increase both the energy and yield of radiation produced in the device, adding to the radiological hazard. Difficulty and cost of adding shielding in the current location along with limitations on frequency of shots has led to plans to relocate the DPF device. Relocation would place the device in an NTS building, which could be dedicated to operating the DPF device with both D-D and D-T reactions.

An intense neutron and gamma source such as the DPF device is an excellent tool for experimental work and is capable of being fired multiple times a day. The radiological hazard from the device is primarily neutrons that can pass easily through the steel walls of a building or trailer and then deposit energy in human tissue. At the current Las Vegas location, clearing the building and reducing the number of shots limits the energy deposited in human tissue, or dose. In order to maximize the potential scientific value of the device, operating the device multiple times a day and several days a week is a must. Realizing this potential while still reducing dose to personnel requires a new location and shielding. The NTS location will provide shielding around the source and locate personnel as far away as feasible from the device.

Bechtel-Nevada is collaborating with UNLV to model potential shielding designs and analyze dose to nearby personnel. The focus of this current work was to provide calculations of dose primarily using the Monte Carlo radiation transport code MCNPX developed by Los Alamos National Laboratory. The code requires the input of geometries, materials and particle types and energies. The Monte Carlo statistics method is then used to transport an individual particle through the geometry and materials. This process is repeated millions of times to predict how an actual radiation source will behave. UNLV operates a 225-node

computer cluster capable of running the MCNPX code in parallel, resulting in an approximately linear speedup factor or a 225-fold decrease in simulation time.

Several potential shielding designs and materials were evaluated. The intended NTS location contains a concrete lined pit with concrete panels as covers. This pit was investigated as a possible location for the device with and without shielding placed over the top. Additionally, floor space is available in the building for shielding to be placed around the device in an above ground configuration. Radiation shielding analysis involves the investigation of configurations of shielding materials, the order of materials, thicknesses, and the actual types of materials used. Investigating shield configurations involves determining the optimal location and placement of shielding around the source that minimizes dose to personnel but still allows for experimental work. The order and thickness of shielding material is important for both the attenuation of the primary radiation and any secondary radiation produced in the shield materials. Choice of materials examines the most cost effective materials that can be used to shield both primary and secondary radiation. Ultimately, the dose to the nearby personnel was calculated for each potential shielding configuration. Two methods of dose calculation, including the conversion of deposited energy to dose and the fluence-to-dose method, were examined.

## CHAPTER 2

### REVIEW OF RELATED LITERATURE

MCNPX is an extension of MCNP4B allowing the transport of all particles and energies, improvement of physics simulations and new variance-reduction techniques as outlined by D. B. Pelowitz in the MCNPX<sup>TM</sup> User's Manual, Version 2.5.0 of April 2005. The use of MCNP in neutron dose calculations behind shielding was validated by Torres et al. at the Applied Physics Division at LANL in "Comparison of MCNP5 and Experimental Results on Neutron Shielding Effects for Materials" in 2004. Agreement between MCNP and experimental neutron dose was excellent and found to be within 5%.

The extensive capabilities of the code make it ideal for radiation shielding calculations. Traditional methods of calculating shielding requirements relied on analytical methods such as those outlined in NCRP Reports No. 51 and 49, published by the National Council on Radiation Protection and Measurements. NCRP Report No. 51 describes basic shielding calculations for neutrons and NCRP Report No. 49 covers X-Ray shielding configurations. Analytical calculations of neutron shielding requirements can be difficult due to the heavy energy dependence of both capture cross sections and dose quality factors, as will be discussed in this work. Scattering of neutrons from shielding materials, walls, the ceiling and other objects can turn a monoenergetic neutron source into a spectrum of energies resulting in difficult and inaccurate hand calculations. The NCRP Report No. 51 suggests

using computer codes such as the Monte Carlo method “for more exact methods of calculating shielding thickness.”

A comparison between analytical methods and the MCNPX Monte Carlo method was reported by U. Titt and W. D. Newhauser in the study “Neutron Shielding Calculations in a Proton Therapy Facility Based on Monte Carlo Simulations and Analytical Models: Criterion for Selecting the Method of Choice” in 2005. This study modeled a complex facility using both MCNPX and analytical methods. MCNPX was found to overestimate dose compared to experimental data. However analytical methods were found to overestimate dose compared to MCNPX by 1.3 to as high as 82.4 times, proving MCNPX to be much more accurate than analytical methods. A Korean study by J. Kim et al. titled “Design of Radiation Shielding for the Proton Therapy Facility at the National Cancer Center in Korea” in 2005 also confirmed that analytical methods overestimated dose compared to MCNPX in a similar facility. Thus, MCNPX has been shown to be more accurate and more efficient than analytical hand calculations.

The code is currently in wide use in many areas of radiation transport and criticality but use with the DPF device as a source term is limited so far. MCNP, the code MCNPX is based on, was used to determine the effects of scattered neutrons on yield measurements for a DPF device of  $10^7$  neutrons per shot, smaller than the DPF in the current study, housed in a narrow concrete corridor. Normally, yield at detectors can be determined from  $1/r^2$  approximations but the narrow corridor caused scatter, requiring Monte Carlo methods. The study by M. Frignani et al. titled “Monte Carlo simulation of neutron backscattering from concrete walls in the dense plasma focus laboratory of Bologna University” used MCNP to optimize neutron detector calibration and placement.

K. Tesch mentions the importance of gamma production in shielding that occurs for neutrons below 25 MeV and in thick concrete shields due to inelastic scattering and capture by hydrogen in the study "A Simple Estimation of the Lateral Shielding for Proton Accelerators in the Energy Range 50 to 1000 MeV." The study comments that gamma dose will be small compared to neutron dose, however the gamma dose for the DPF device in the current study will be investigated.

While no experimental data on the X-rays produced in the current DPF device is available yet, a study used radiographic film to measure X-ray energy from a DPF device located in Chile. The study titled "Determination of the Effective Energy of Pulsed Powerful Hard X-Ray Sources based on Pinch Plasma Focus Discharges" by V. Raspa et al. measured X-rays with energies from 80-110 keV generated in the plasma by Bremsstrahlung from thermal electrons and also collision of high energy electrons with the anode material.

A dense plasma focus device is in operation at Texas A&M University, producing  $10^{11}$ - $10^{12}$  D-T neutrons and shielded by concrete block and 60cm of concrete. The neutron yield of the device along with low and high pressure operating modes are discussed in the article "Neutron Emission Characteristics of a High-Current Plasma Focus: Initial Studies" by B. L. Freeman, et al. of Texas A&M along with E. C. Hagen and L. Ziegler of Bechtel Nevada. Additionally, a good description of the operation of a DPF device with a yield similar to that of the current device is given by M. Scholz et al. in the report "X-Ray and Neutron Emission from PF-1000 Facility."

## CHAPTER 3

### THEORY

Several principles must be examined in order to understand the concepts behind radiation shielding and dose analysis for the DPF device. This section covers these necessary principals in understanding the basics of radiation, why this radiation presents a radiological hazard to humans, how the DPF device produces radiation, how that radiation can be shielded and finally how the shielding is evaluated.

#### 3.1 The Fundamentals of Radiation

Radiation is categorized as non-ionizing and ionizing radiation. These terms refer to the capability of the radiation to excite or strip electrons from materials. Non-ionizing radiation is generally low energy that is incapable of removing an electron from an atom, such as radio waves or microwave radiation. Only radiations with energies higher than that of ultraviolet are usually considered ionizing and present a hazard to biological organisms. The shield design must limit the amount of energy that ionizing radiation, produced in the DPF device, deposits in the tissue of nearby workers.

Ionizing radiation is further broken down into directly ionizing radiation and indirectly ionizing radiation. Charged particles such as electrons, protons, alphas and heavy ions are considered directly ionizing. These particles carry a charge and can directly strip

electrons from atoms as they pass through matter via electromagnetic interactions. Because they carry a charge, these directly ionizing radiations will continually slow down as they pass through matter as their energy is gradually lost by Coulombic interactions with the electrons in the material. Charged particles undergo many interactions since a typical interaction results in only a small kinetic energy loss. Heavy particles travel in a relatively straight path while light particles, such as electrons, can travel in a very nonlinear path due to their much smaller mass.

Indirectly ionizing radiation consists of uncharged particles like neutrons, gamma and x-rays. These types of radiation must first interact with an electron or nucleus to deposit energy and do not experience continual slowing down in matter like charged particles. Neutrons, which are uncharged or neutral particles, were of particular concern in the current problem since they are a primary radiation produced in the DPF device. Rather than charged particles, which experience a continuous slowing down, the uncharged neutron can only deposit energy through collisions with the nucleus. The probability of neutron interaction is quantified by the cross-section, or the Greek symbol sigma  $\sigma$ , and typically given in units of  $\text{cm}^2$  or "b" for barns ( $\text{b}=10^{-24}\text{cm}^2$ ). Neutrons are often labeled based on their energies. "Thermal" neutrons have energies less than 0.5 eV, "intermediate" neutrons have energies between 0.5 eV and 10 keV, and "fast" neutrons have energies above 10 keV.

The amount of energy possessed by radiation is most often referred to in terms of keV or MeV meaning one thousand electron volts and one million electron volts, respectively. An electron volt, labeled eV, is equal to  $1.602 \times 10^{-19}$  Joules and is the amount of kinetic energy possessed by an electron after being accelerated across a one volt potential.

Neutrons interact through a variety of methods. Elastic scattering is scattering that results in no kinetic energy gain by either the nucleus or scattered neutron. Inelastic scattering between a neutron and a nucleus results in the nucleus being left in an excited state. The excited nucleus subsequently decays by emission of a gamma ray. Since the process is endothermic, a threshold energy for the neutron is necessary for the nucleus to reach its first excited state. The terms low-Z and high-Z refer to the number of protons in the nucleus. Heavier atoms have more protons and thus are high-Z with a corresponding Z number of electrons, while light atoms such as hydrogen with one proton are low-Z. The threshold for inelastic scattering is higher for low-Z material since excited states have large energy requirements. Conversely, a lower threshold is required for high-Z material since excited states have smaller energy requirements. As a result of these thresholds, neutron interactions in low-Z material will primarily be elastic while interactions with high-Z material will be inelastic.

Another type of neutron interaction important to shielding applications is radiative capture, often labeled as  $(n,\gamma)$  reactions. In this exothermic interaction, a gamma ray is emitted from the nucleus after the neutron is captured. Thermal neutrons with low energies have the highest cross-section for interaction by radiative capture. This type of interaction is important in shielding because of the resulting gamma ray. A low energy neutron with less than an eV of energy can be captured by a nucleus with subsequent emission of a gamma ray of several MeV.

Neutron interaction can also occur by charged particle production. In this endothermic process, a neutron is captured by a nucleus resulting in the emission of a charged particle such as a proton labeled  $(n,p)$ . Due to the short range of most charged

particles, this interaction is not as great a concern in shielding but is of great importance when calculating dose in human tissue. Other neutron interactions, such as production of neutrons in  $(n,2n)$  reactions have very small cross-sections. Fission by neutrons is not considered in the current situation.

Gamma rays and x-rays are fundamentally the same since both are photons or electromagnetic radiation. The source of the photon differentiates whether it is called a gamma ray or x-ray. Gamma rays are emitted from the nucleus of an atom after it is excited by an interaction or left in an excited state after decay and also by annihilation between an electron and positron. X-rays result from charged particles changing energy levels, such as orbital electrons, or when charged particles decelerate. For our purposes, both gamma rays and x-rays will simply be referred to as either gamma rays or photons. Like neutrons, gamma rays are uncharged and do not experience a continuous slowing down in matter. Instead, gamma ray range is statistical and follows a probability of interaction using cross-sections like neutrons. The primary methods for energy deposition from gamma rays are photoelectric absorption, Compton scattering, pair production and photonuclear reactions. The method or methods a gamma ray interacts depends on both the gamma energy and the  $Z$  of the material.

The photoelectric effect is the dominant interaction method for low energy photons. In this process an incident gamma ray removes a bound electron when that gamma ray has sufficient energy. The gamma ray deposits all of its energy to the medium by this method. The incident gamma ray must have enough energy to match the binding energy of the electron in order for that electron to be ejected. The cross-section for the photoelectric effect is strongly dependent on the  $Z$  of the material and the energy of the gamma ray, being larger

at higher  $Z$  and smaller energies. This proportional relation is shown in equation 3.1 with  $Z$  the number of electrons of the atom,  $E$  the energy of the gamma ray and  ${}_a\tau$  the cross-section or probability of photoelectric absorption.

$${}_a\tau \propto \frac{Z^4}{E^3} \quad \text{Eq. 3.1}$$

For medium gamma ray energies, the Compton effect dominates. Additionally, the Compton effect will dominate over a large energy range (~20 keV to 30 MeV) for low- $Z$  material such as human tissue. Photons deposit energy in the Compton effect by scattering from an orbital electron, resulting in the emission of the scattered electron and the original photon. The relation between original photon energy  $E_o$  and the scattered photon energy  $E'$  is presented in equation 3.2 where  $\theta$  is the angle of scatter of the photon after interaction:

$$E' = \frac{E_o}{1 + \left(\frac{E_o}{0.511 \text{ MeV}}\right) (1 - \cos \theta)} \quad \text{Eq. 3.2}$$

At gamma ray energies above 1.022 MeV and in higher- $Z$  material, pair production becomes a dominant effect over the Compton Effect. Pair-production occurs when a photon essentially disappears in a Coulomb field and forms an electron and positron. A positron is a positively charged electron with identical mass but opposite charge. The threshold for this reaction is 1.022 MeV since the rest mass of a positron and an electron are both 0.511 MeV according to Einstein's  $E=mc^2$ . Therefore, the incident photon must possess enough energy to

be converted into the mass of the two particles. The energy dependency of these interaction types can be seen subsequently in figure 3.6, a photon cross-section plot for lead.

### 3.2 Theory of Health Physics

Health physics deals with the effects of ionizing radiation in human tissue. Dose to tissue is quantified as energy deposited per unit mass. The SI unit for dose is the gray or Gy with  $1 \text{ Gy} = 1 \text{ J/kg}$ . The non-SI unit for dose is the rad with  $1 \text{ rad} = 0.01 \text{ Gy}$ . Ionizing radiation deposits energy in tissue by charged particles. Indirectly ionizing radiations, such as gamma rays and neutrons, deposit energy by creation of charged particles that subsequently interact with tissue.

Since most of the human body is water, a large portion of energy from charged particles results in the ionization and excitation of water molecules. The nitrogen found in human tissue can also lead to proton production from neutron exposure as will be examined in this work. The ionization and excitation of water molecules leads to the damage of cell DNA. While some damage to DNA can be repaired, cell death can occur along with mutations into cancerous cells. How effective a particular radiation is at killing cells allows us to apply a quality factor when calculating dose. Quality factors are shown in Table 3.1.

Type of Radiation	Quality Factor Q
X-Ray, gamma, or beta radiation	1
Alpha particles, multiple-charged particles, fission fragments and heavy particles of unknown charge	20
Neutrons of unknown energy	10
High-energy protons	10

Table 3.1 Quality Factors for Radiations from NRC Regulation 10CFR20

These quality factors can range from 1 to 20 depending on particle type and energy. Neutrons of known energies are further broken down by energy and have quality factors ranging from 2 to 11. Calculations of dose from neutrons in this work use Table 3.2 quality factors. Multiplying Gy or rad by a quality factor results in the dose equivalent term Sievert (Sv) for SI units or the rem in non-SI units. In this study, a mrem or 1/1000 of a rem was used when discussing dose. For reference, the average background dose to humans from natural and manmade sources is about 360 mrem per year. A limit of 100 mrem per year of exposure from the device is desired which is well below federal regulations. For reference, a lethal acute dose of radiation would be about 500 rems.

<b>Neutron Quality Factors</b>	
<b>MeV ranges</b>	<b>Q</b>
0 to 1E-3	2
>1E-3 to 1E-2	2.5
>1E-2 to 1E-1	7.5
>1E-1 to 1	11
>1 to 2.5	9
>2.5 to 5	8
>5 to 7	7
>7 to 10	6.5
>10 to 14	7.5

Table 3.2 Quality Factors for Neutrons of Known Energies

Dosimetry of radiation sources is based on the amount of energy that is actually deposited in tissue. This can be done by Monte-Carlo methods in MCNPX using tissue equivalent phantoms. These phantoms represent human tissue and allow calculation of energy deposited by each radiation type. This energy deposition can then be converted to Sv or rems using appropriate quality factors. Another method of performing dose calculations is

converting from flux to dose using conversion factors. Neutron dose  $D_n$  from elastic collisions is given by equation 3.3.

$$D_n = [E_{tr} \sigma_s \left(\frac{N_v}{\rho}\right)] \Phi_n \quad \text{Eq. 3.3}$$

Where  $E_{tr}$  is energy transferred to the scattered nucleus in MeV,  $\sigma_s$  is the elastic scattering cross-section in  $\text{cm}^2$ ,  $N_v$  is atom density in  $\text{atoms}/\text{cm}^3$ ,  $\rho$  is the density of the material in  $\text{g}/\text{cm}^3$  and  $\Phi_n$  is the incident neutron flux in  $\text{neutrons}/\text{cm}^2$ . This results in  $\text{MeV}/\text{g}$  which can be converted to  $\text{J}/\text{kg}$  and then Gy or rad using the conversion  $1 \text{ MeV}/\text{g} = 1.602 \times 10^{-10} \text{ J}/\text{kg}$ .

Dose from a gamma ray emitted during neutron scattering or capture  $D_{n-i}$  is represented by equation 3.4:

$$D_{n-i} = [E_\gamma AF_\gamma \sigma_\gamma \left(\frac{N_v}{\rho}\right)] \Phi_n \quad \text{Eq. 3.4}$$

Where  $E_\gamma$  is the energy of the gamma emitted,  $\sigma_\gamma$  is the cross-section or probability of the interaction occurring and  $AF_\gamma$  is the percentage of energy deposited in the body by that gamma (dependent on gamma energy).

Similarly, the dose  $D_\gamma$  from gamma rays can be represented by:

$$D_\gamma = [E_\gamma \left(\frac{\mu_{en}}{\rho}\right)] \Phi_\gamma \quad \text{Eq. 3.5}$$

Where  $E_\gamma$  represents the incident gamma energy in MeV,  $\mu_{en}$  is the mass energy absorption coefficient for the material in  $\text{cm}^2/\text{g}$  and  $\Phi_\gamma$  is the incident gamma flux in gammas/ $\text{cm}^2$ .

Production of charged particles by neutron capture is also important in dosimetry as the quality factors for protons and alphas make them more destructive than gamma rays. Neutron capture with charged particle production dose (in this case a proton that does not leave the target volume)  $D_{n-p}$  is represented by:

$$D_{n-p} = [Q_{event} \sigma_{event} \left(\frac{N_v}{\rho}\right)] \Phi_n \quad \text{Eq. 3.6}$$

Where  $Q_{event}$  represents the Q-value of the reaction or the energy released in MeV,  $\sigma_{event}$  represents the probability for the event in  $\text{cm}^2$  and  $\Phi_n$  represents the incident neutron flux.

Charged particle dosimetry is slightly different due to the continually slowing down nature of charged particles in matter. The stopping power in MeV/g of charged particles is often given and represents an instantaneous rate of energy loss in a material. Stopping power increases as a charged particle begins to slow down. Since a slow particle spends more time near each atom it can deposit more energy in a certain distance. A good approximation for dose rate  $H_e$  in rem/hr from a uniform electron beam of energy 1 to 200 MeV of flux  $\Phi_e$  in  $\text{cm}^2/\text{s}$  is represented by equation 3.7:

$$H_e = 1.6 \times 10^{-4} \Phi_e \quad \text{Eq. 3.7}$$

Dose calculation methods such as equations 3.3 through 3.6 must be done for every interaction a neutron or gamma undergoes and also for every secondary particle produced. The dose from electrons with equation 3.7 is a rule of thumb and only applicable for uniform electron irradiation. As mentioned, cross-section values for interactions of neutrons and gammas change as the incident particle energy changes. Because of the impracticality of doing these calculations for a neutron or photon beam that covers a large spectrum of energies, simple flux-to-dose conversion factors or Monte-Carlo techniques like MCNPX are used. Direct flux-to-dose conversion factors tend to overestimate dose as compared to using MCNPX and energy deposition calculation. For completeness, both methods were examined and compared in this work. The Monte-Carlo method of radiation transport using MCNPX is presented in further detail in subsequent sections.

### 3.3 How the Dense-Plasma Focus Device Functions

The production of neutrons in the DPF is the result of a fusion reaction by the creation of a plasma. At room temperature, deuterium gas exists as a diatomic molecule  $^2\text{H}_2$  with an average thermal energy of 0.025 eV. By passing an electrical current through the gas, the deuterium gains energy and becomes both ionized with the stripping of electrons and atomized with the breaking of the molecules into individual atoms. At this point the gas becomes a plasma of about 100,000 °F where fusion between atoms can begin. The high temperature of the gas means that repulsion between nuclei is overcome. Fusion reactions result in a release of energy since part of the mass of the nuclei is converted to energy, following Einstein's  $E=mc^2$  relation.

A dense plasma focus (DPF) device accelerates electrons to high velocities inside a gas, resulting in a short-lived plasma with a lifetime of a few microseconds. This acceleration is facilitated using capacitor banks capable of producing a large potential difference between an anode and cathode. The circular cathode surrounds an inner circular anode with a gas in between. The plasma moves up the device and a shockwave produces very dense plasma, allowing fusion, which then breaks up at the top of the anode. During this breakup, electrons and bremsstrahlung gamma rays are emitted. A conceptual layout of a DPF is shown in figure 3.1 with the plasma shockwave shown progressing from 1 to 3 and finally the focus point at 4.

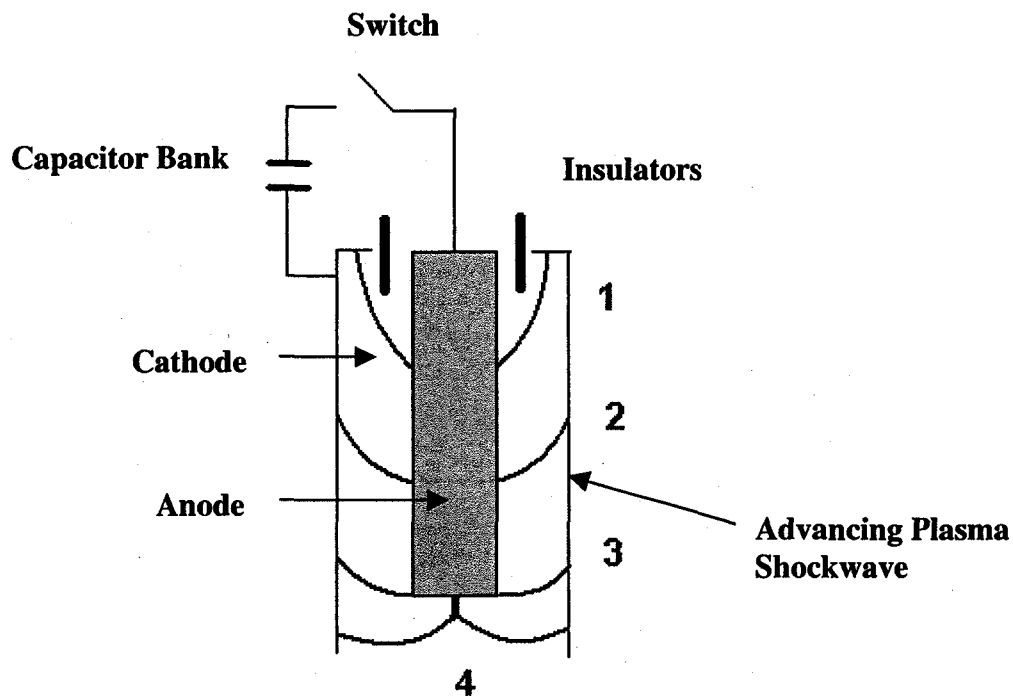


Figure 3.1 Schematic Drawing of DPF Assembly and Plasma Progression

The actual DPF device currently located in North Las Vegas is shown in figure 3.2 while being assembled. One can see the outer copper cathode and inner anode with the pinch occurring at the bottom for this assembly. The gas, composed of deuterium and tritium if D-T fusion is desired, is contained around the anode and cathode with the lower pressure vessel. Current operational configuration of the DPF device and the capacitor bank at the North Las Vegas location is shown in figure 3.3.

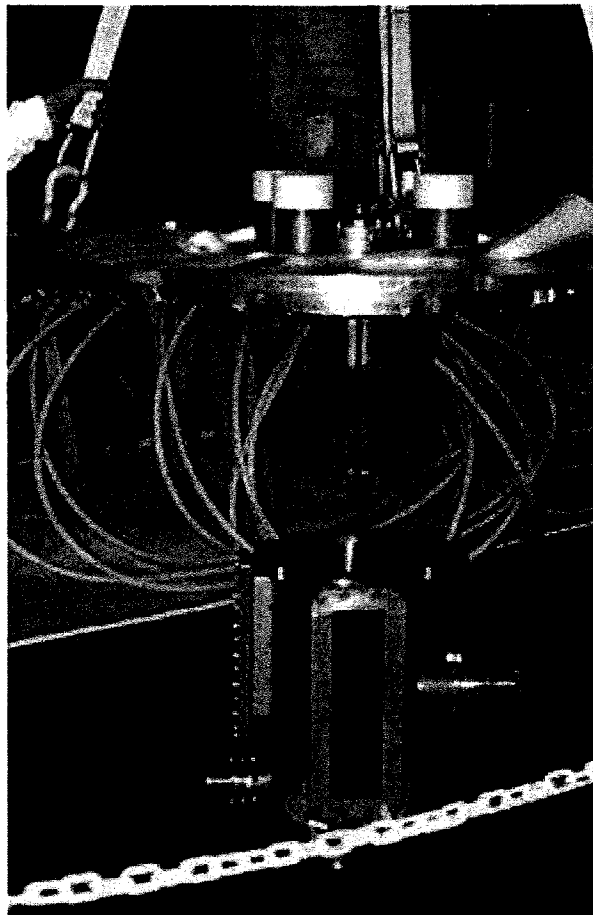


Figure 3.2 DPF Anode, Cathode and Vacuum Chamber Assemblies

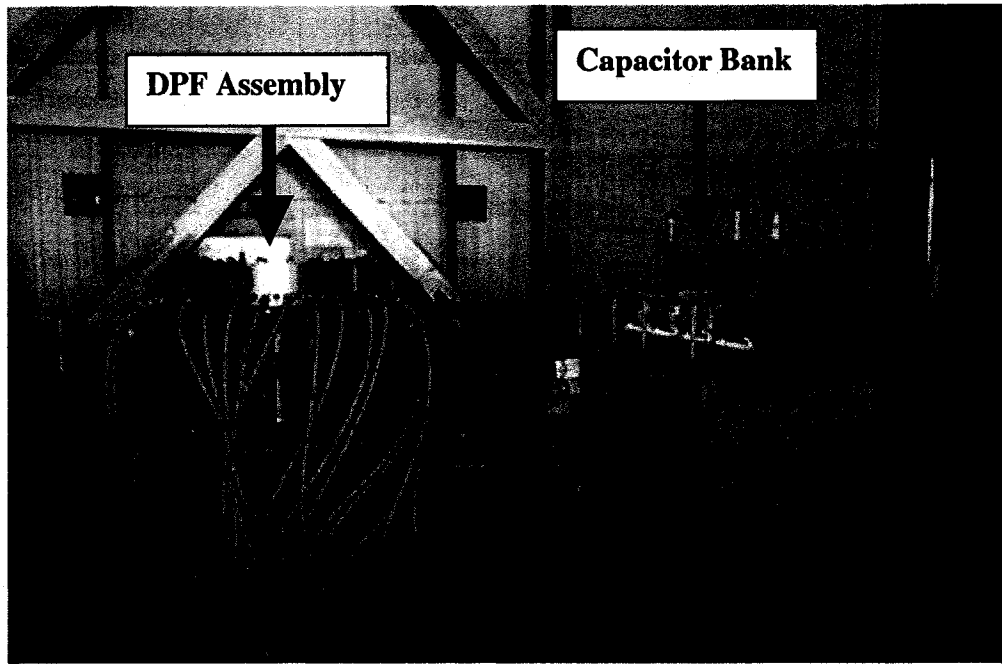


Figure 3.3 DPF Assembly and Capacitor Bank at Current Location

The DPF device can operate with either the deuterium-deuterium (D-D) reaction described or deuterium-tritium (D-T) reactions. Deuterium is hydrogen with an extra neutron while tritium is hydrogen with two extra neutrons. Two possible reactions exist for the fusion of deuterium and deuterium. The neutron producing D-D reaction with  $^2\text{H}$  as deuterium,  $^3\text{He}$  as tritium and  $n$  as a neutron is represented by equation 3.8:



Where the 3.3 MeV is kinetic energy carried by both the He-3 and neutron. The neutron carries an average of 2.45 MeV with the He-3 carrying the remainder. The energy spectrum produced in the D-D reaction is presented in figure 3.4. This spectrum was produced by MCNP with the peak at 2.45 MeV from D-D fusion neutrons producing fission in a surrounding shell of uranium.

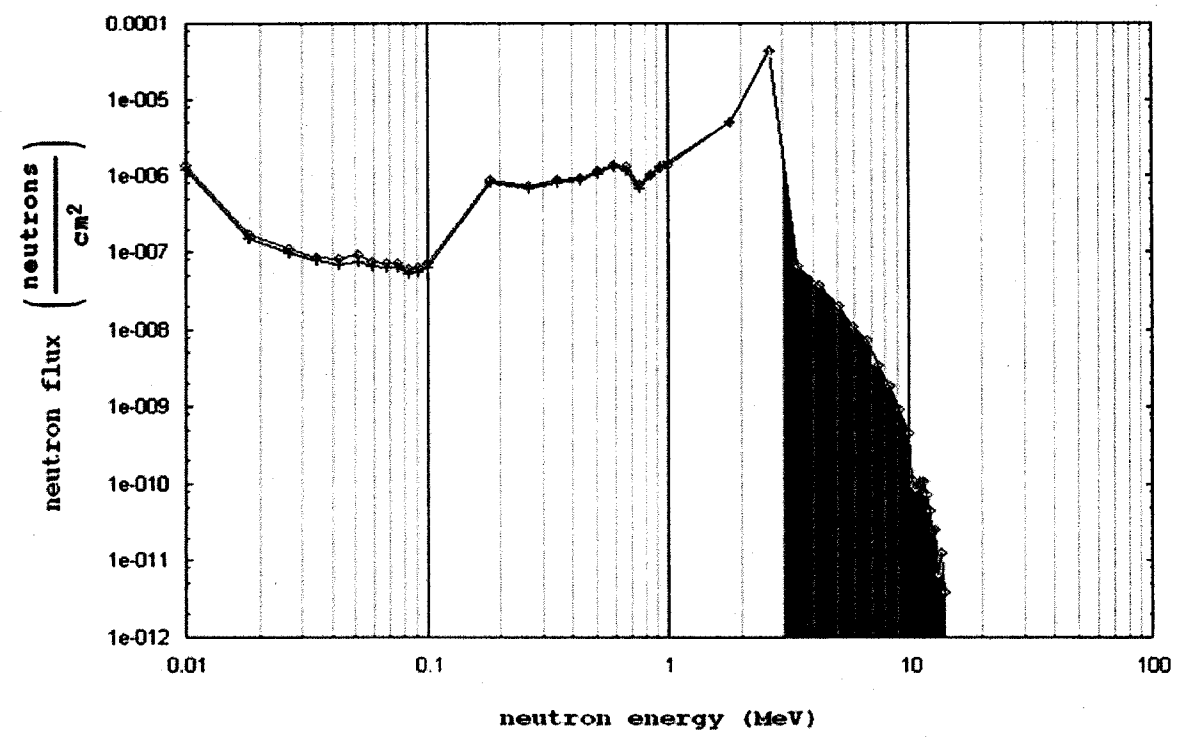


Figure 3.4 Neutron and Uranium Spectrum from D-D Reaction

The other possible D-D reaction with  $^3\text{H}$  as tritium and p as a proton is represented by equation 3.9 with the tritium and proton carrying 4.0 MeV. The probability of the neutron and proton producing reactions of equation 3.8 and 3.9 are approximately equal.



Operating the DPF device with the D-T reaction results in a larger energy yield. With  $^3\text{H}$  as tritium, this reaction is represented by equation 3.10:



Where the 17.6 MeV is kinetic energy carried by both the  $^4\text{He}$  and the neutron. The neutron carries an average energy of 14.1 MeV with the remainder carried by the He-4.

In both the D-D and D-T reactions, the neutron is the particle of concern for shielding purposes along with gammas. Gammas are produced through bremsstrahlung deceleration of both electrons and ions in the plasma. The proton produced in equation 3.9 has an energy of about 3 MeV, resulting in a range in copper of around 2 mm. Therefore the proton will not pose a radiological threat near the device. Likewise, the He-3 and He-4 do not have sufficient range, only a few cm in air, to pose a radiological threat.

### 3.4 Theory of Radiation Shielding

Because the current location for the device has no shielding, operation is limited due to the radiological hazard of the neutron and gamma radiation. Shielding at the new location will reduce dose received by personnel and allow more frequent use. In order to reduce dose, we must place people as far away as possible or provide adequate shielding. Putting large distances between personnel and the device can be impractical when frequent firing of the device is necessary. The current work will therefore place the personnel operating the device as far away as practical and construct shielding to further reduce exposure to radiation.

The easiest way to reduce dose is to put distance between oneself and the radiation source. This concept is represented by the uncollided flux  $\Phi_u$  of uncharged particles, or particles that reach a point without interaction along the way, at a point distance  $r$  from a radiation point source as presented in equation 3.11.

$$\Phi_u = \frac{S_o}{4\pi r^2} \quad \text{Eq. 3.11}$$

Where  $S_o$  is the source strength in particles emitted per decay per second. One can see that the flux falls off as  $1/r^2$  and so doubling the distance to the source reduces flux by a factor of four. Placing shielding between oneself and the source further reduces flux by an exponential amount as in equation 3.12.

$$\Phi_u = \frac{S_o}{4\pi r^2} e^{-\mu x} \quad \text{Eq. 3.12}$$

Where  $\mu$  is the attenuation coefficient for the shielding material in 1/cm and  $x$  is the shield thickness in cm. Note that both equations 3.11 and 3.12 ignore the small attenuation in air and apply strictly to uncharged radiations. As discussed previously, charged particles like electrons undergo a continual slowing down and will not be present beyond a certain range in air. Additionally, caution is required when using equation 3.12 as will be discussed shortly.

When selecting shielding material, one must consider both the primary radiation types and secondary radiation that may be produced in the shield. In the current work, we had neutrons and gammas as a primary source. Neutrons are best shielded through “downscattering” or scattering the neutron in the shield until it reaches sufficiently low energies. The downscattering of neutrons is most effective in very low-Z material. Ideally, this material will be very hydrogenous, meaning it contains a large fraction of hydrogen. The average energy transferred  $T_R$  to a recoil atom by a neutron is represented in equation 3.13.

$$T_R = \frac{1}{2} \left[ 1 - \left( \frac{A-1}{A+1} \right)^2 \right] T_n \left[ 1 + \frac{Q}{T_n} \left( \frac{A+1}{2A} \right) \right] \quad \text{Eq. 3.13}$$

Where  $T_n$  is the energy of the incident neutron,  $Q$  is the energy released in the reaction and  $A$  is the atomic number of the atom. One can see for hydrogen with atomic number  $A=1$  that equation 3.13 becomes a maximum. Therefore neutron scattering in hydrogen will result in the largest average energy transfer loss by the neutron per collision.

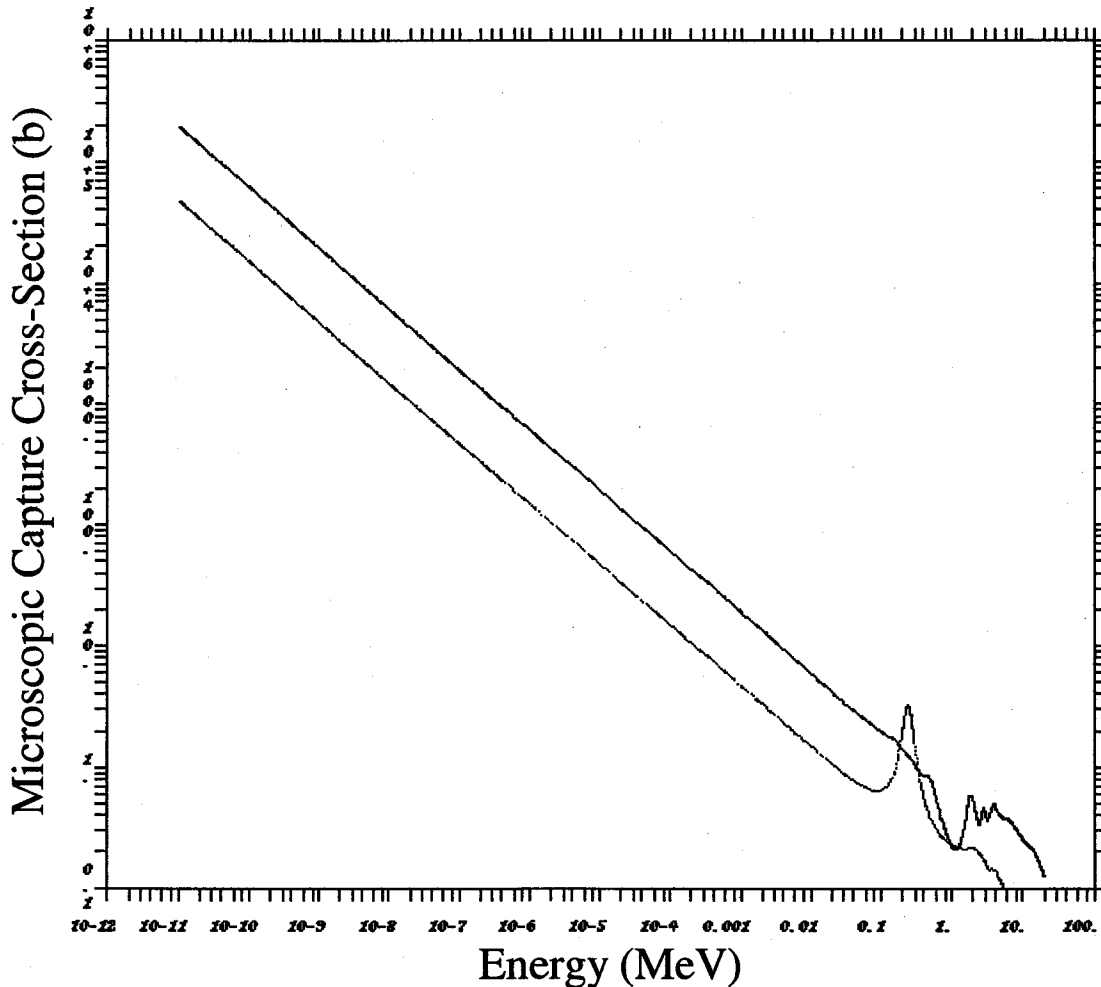


Figure 3.5 B-10 (top) and Li-6 (bottom) Neutron Capture Cross-Sections (MCNPX)

Reducing the energy of neutrons is essential to reducing dose. One can see from table 3.2 that low energy neutrons have the smallest quality factor for dose. Additionally, thermalized neutrons are more easily absorbed by radiative capture, which eliminates them as

a hazard. Certain materials are commonly used to capture thermalized neutrons, including the boron isotope B-10 and lithium isotope Li-6. The cross-section for neutron absorption increases with decreased neutron energy as one can see in figure 3.5.

While radiative capture eliminates the neutron as a hazard, a high-energy gamma is produced in this exothermic reaction and may also need shielding. For example, thermal neutron capture in B-10 produces a gamma with up to 11.447 MeV of energy. One method of shielding both neutrons and gamma rays produced in capture is to use low-Z hydrogenous material doped with an isotope such as boron and follow that shield with a high-Z material to attenuate gammas produced in the capture reactions.

Gamma shielding relies on the exponential attenuation provided by the shielding material used. Generally, high-Z materials are desirable as these have the largest  $\mu$  values due to the large number of electrons present per atom. The effectiveness of gamma shielding is often given in terms of “half value layers” or the thickness of material required to reduce the gamma intensity to  $\frac{1}{2}$  of the original intensity. The half value layer value, or HVL, is presented in equation 3.14 with units of cm for a material with attenuation coefficient  $\mu$  in  $\text{cm}^{-1}$ :

$$HVL = \frac{\ln 2}{\mu} \quad \text{Eq. 3.14}$$

Consequently, high-Z materials with larger attenuation coefficient  $\mu$  will have a smaller HVL and require less material for shielding. Following a low-Z hydrogenous neutron shield with a high-Z gamma shield to provide sufficient half value layers is a

common practice for eliminating capture gamma rays as a radiological hazard. The cross-section for one such high-Z material, lead, is illustrated in figure 3.6 showing the three major interactions and the total.

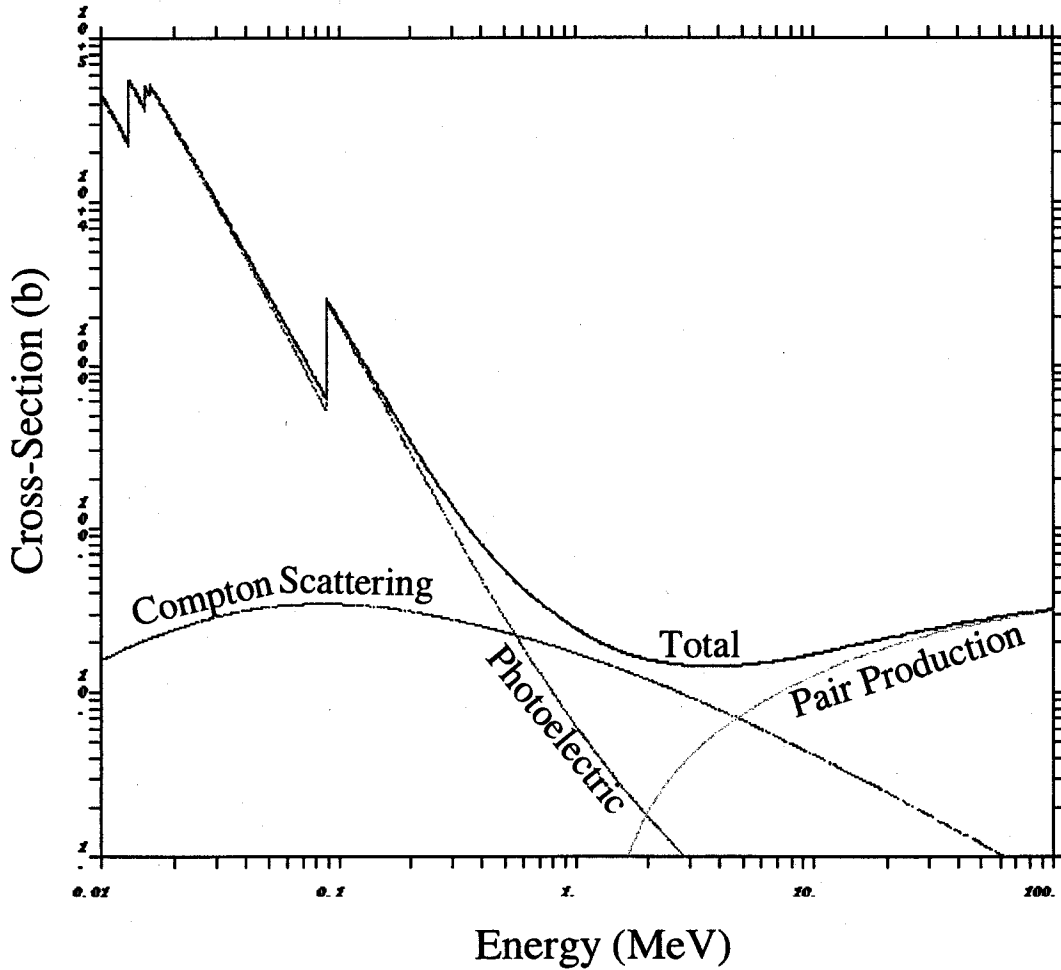


Figure 3.6 Photon Cross-Sections for Lead (MCNPX)

Shielding neutrons and gammas also requires that one account for “buildup” of radiation in the shield, or scattered and secondary radiation that escape the shield and contribute to dose. The exponential attenuation in a shield for uncharged radiation shown in equation 3.12 does not account for scattered radiation or secondary radiation. Scattered

radiation is that which interacts with matter in the shield but is not absorbed. This scattered radiation can still leave the shield. Multiplying equation 3.12 by a unitless “buildup factor” B results in equation 3.15:

$$\Phi_{\gamma} = B \frac{S_o}{4\pi r^2} e^{-\mu x} \quad \text{Eq. 3.15}$$

The buildup factor B can vary greatly depending on the shielding material used and the thickness of the shield. Buildup factors for gamma rays can be as high as  $10^2$  in a thick shield of concrete due to the large number of lower energy photons created through interactions in the material. The following example illustrates the effect of buildup factors and the advantage of MCNPX to automatically account for buildup. A beam of gammas is incident on a slab of lead shielding as illustrated in figure 3.7.

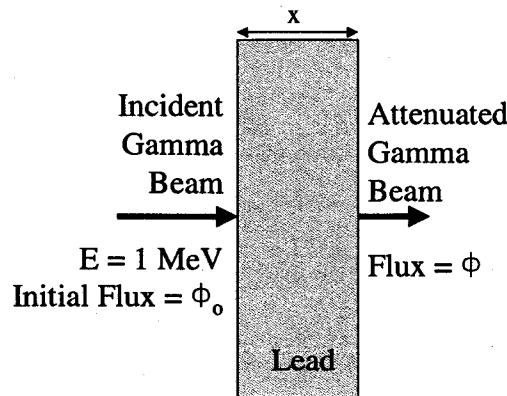


Figure 3.7 Gamma Beam Attenuation Example

Since the example shown in figure 3.7 is a beam, the intensity does not fall off with distance as  $1/4\pi r^2$  and so equation 3.15 becomes equation 3.16:

$$\Phi_o = B \Phi e^{-\mu x} \quad \text{Eq. 3.16}$$

For the example, lead was used as a shield which has a total photon cross-section from figure 3.6 of about 24.3 barns, corresponding to an attenuation coefficient  $\mu = 0.801 \text{ cm}^{-1}$  and we choose a shield thickness  $x$  equal to 1 HVL. Using equation 3.14, a HVL for lead equals 0.865 cm. With  $x = 0.865 \text{ cm}$ , or one half value layer, in equation 3.16 and assuming no buildup factor ( $B=1$ ) we calculated a flux at the back of the shield of half the original intensity as shown in table 3.3.

	<b>Hand Calculation</b>	
	<b>With B=1</b>	<b>MCNPX</b>
<b>Initial Flux <math>\Phi_o</math> (photons /cm<sup>2</sup>)</b>	<b>10</b>	<b>10</b>
<b>Final Flux <math>\Phi</math> (photons/cm<sup>2</sup>)</b>	<b>5</b>	<b>7.09 +/- .01</b>

Table 3.3 Hand Calculation and MCNPX calculation of Flux in Figure 3.7

MCNPX can account for all scattered photons that make the flux behind one half-value layer of shielding about 42% higher than predicted by hand. Without a Monte-Carlo radiation transport code like MCNPX, we would need to use tables to determine the buildup factor  $B$  and it would only be accurate for simple geometries.

Just as with gammas, we must deal with buildup in neutron shielding. The secondary radiation created through neutron capture can oftentimes be more hazardous than the primary neutrons. Neutron cross-sections vary greatly depending on neutron energy and material composition. A small change in material or energy can result in a large change in the neutron intensity. Due to these variables, using a simple buildup factor  $B$  for neutrons like what is used for gammas is oftentimes impossible. Situations where a simple neutron buildup factor can be applied are very restricted. In circumstances such as the current problem, where shielding consists of multiple materials and where geometries are not simple arrangements, the use of buildup factors for neutrons in hand calculations are ineffective. The most efficient way to determine neutron and gamma flux around the DPF device shield is through the use of Monte Carlo methods such as MCNPX.

### 3.5 Theory of MCNPX

MCNPX is a Monte-Carlo radiation transport code developed at Los Alamos National Lab. The code is the latest generation of Monte Carlo transport codes that have been in development at LANL for almost 60 years. UNLV is part of the beta test team for the code and we have access to the latest versions. The code is installed and run on both individual computers and a dedicated 225-node Beowulf cluster. This cluster allows MCNPX to be run in parallel on all 225 processors, resulting in an approximately linear speed up. A portion of the UNLV Beowulf cluster is pictured in figure 3.8. The speedup factor from parallel processing combined with variance reduction techniques can allow very large or complicated geometries to be simulated in reasonable amounts of time. The current problem is one such geometry with a large building, trailer and significant distances involved. Achieving reliable

results for such large geometries would be difficult, if not impossible, without the speedup factors gained by parallel processing and variance reduction.



Figure 3.8 225 Processor Beowulf Cluster at UNLV

The Monte-Carlo method of radiation transport involves transporting one particle at a time through materials configured in geometries specified by the user. MCNPX requires the user to build an “input deck” containing the sizes and locations of shapes along with their material composition. A sample input deck is included in Appendix I along with an output deck in Appendix II. The user also inputs the type of radiation source and its location. An illustration of the transport of photons in MCNPX is presented in figure 3.9. Particles are transported statistically from the source in random directions through materials where the physics of each interaction is predicted using tabulated experimental data or physics models.

An individual particle is started at the source and followed until it is absorbed or when it reaches an area where it is not necessary to track anymore, such as a problem boundary.

Figure 3.9 shows an example of photon interactions in a material.

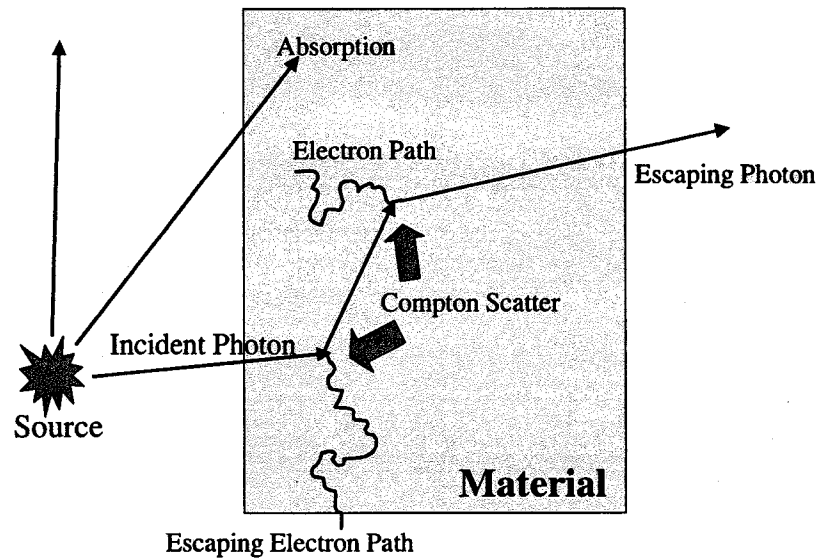


Figure 3.9 Example of MCNPX Transport of Radiation Through Materials

Each small distance traveled in the material, the probability of an interaction is calculated according to known experimental cross-sections that are stored in tables. When experimental data is not available, MCNPX can use physics models to determine interaction probabilities, though this capability was not necessary for this problem. If an interaction does occur then MCNPX calculates the energy of the scattered particle or particles according to known equations, such as the Compton Effect relation of equation 3.2, and continues to transport that particle and any secondary particles. After the particle is totally absorbed or leaves the problem volume, MCNPX then starts another new particle from the source and

performs the same transport process. This is repeated as many times as necessary, oftentimes with millions of particle tracks, until a statistically reliable answer is achieved.

MCNPX is able to create and track all secondary particles produced by both charged and uncharged radiation, account for buildup factors as illustrated previously, accurately model complex geometries and also track the energy deposited in materials and the flux at various locations. These features make Monte Carlo methods far superior to analytical calculations for the current work.

## CHAPTER 4

### METHODOLOGY

The ultimate goal of shielding for the DPF device is the reduction of dose to personnel near the device in accordance with the ALARA concept, or as low as reasonably achievable. The DPF device is a prolific source of high-energy neutrons along with gamma radiation. While these types and amounts of radiation are useful for experiments, they present a radiological hazard to the personnel operating the device and carrying out experiments. Total elimination of dose to personnel cannot be achieved without placing the device in a very remote location. Additionally, the device must be accessible for both experimental use and maintenance. Therefore we must provide enough shielding to reduce dose to nearby personnel to a safe level while still retaining functionality of the device. Shielding for the device must be effective and not cost prohibitive. Several shielding geometries were examined along with potential materials. Both the thicknesses and order of materials are important in reduction of dose. Additionally, two different methods of dose calculation were examined.

#### 4.1 The DPF Device as a Radiation Source

Accurate MCNPX simulations require the input of a source term representing the radiation emitted. Both the plasma created in the DPF device and the possible fusion

reactions emit large amounts of radiation. The fusion produced neutrons and the gamma rays from the plasma breakup are of primary concern. Fusion occurs at the focus point at the bottom of the anode (figure 3.1) and can be modeled for our purposes as a point source of radiation. Maximum possible neutron yields were assumed for our models in order to represent a worst-case scenario. For D-D reactions, dose was calculated as if the point source were to emit  $10^{11}$  neutrons of 2.45 MeV. In the D-T reaction, we used a yield of  $10^{13}$  neutrons of 14 MeV.

## 4.2 Shielding Configurations

Functionality of the device as an experimental tool is a major requirement when designing shielding configurations for the device. Since most experiments require a direct line of sight (LOS) to the focus point with no shielding materials obstructing the view, total enclosure of the device is not feasible. Additionally, shielding must allow personnel to access the device for routine maintenance and also allow the device to be moved out of the shielding for upgrades, alterations or other modifications. An existing crane in the NTS building provides more options as heavy shielding material and/or the DPF device can be lifted and placed into position. A concrete lined pit also exists at the NTS building and offers another potential shielding option. Several potential shielding configurations that vary in cost and versatility are presented here. These shields will be varied in material thickness and in arrangement of materials.

The first shield configuration to be modeled is the simple square shield shown conceptually in figure 4.1. This configuration provides excellent dose reduction since radiation must pass through shielding material to reach personnel or scatter from the ceiling.

The obvious downside of this configuration is limited LOS operation since experiments must be placed inside the shield. Maintenance of the device is also difficult since personnel must climb over shielding material to reach the device. Additionally, the DPF device must be lifted or shielding material removed in order to allow movement of the device out of the shield.

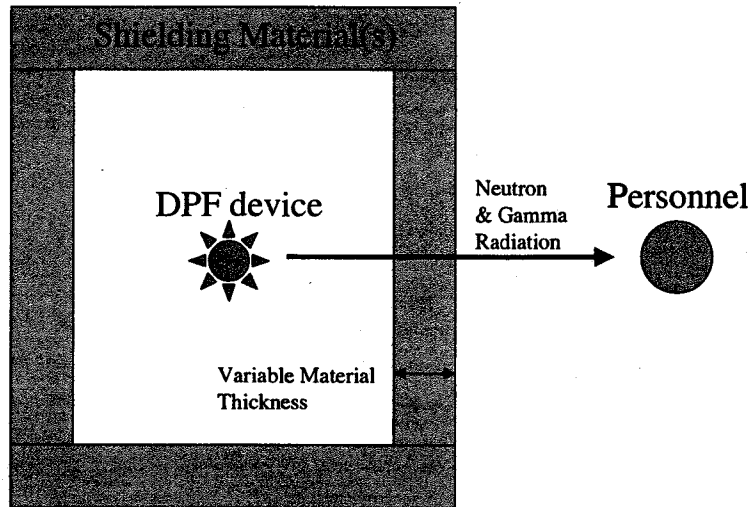


Figure 4.1 Simple Square Shield Concept for Radiation Attenuation

Increasing the functionality of the square shield results in the “labyrinth” configuration. The labyrinth is presented in figure 4.2. This configuration allows more versatility as the device can be moved in and out of the shielding easily in addition to allowing easy access by personnel and scientists. LOS operation is still limited however as experiments must be placed close to the device. An additional advantage of the labyrinth is that one side offers three layers of shielding protection. However, radiation can still leave the shield by scattering from the ceiling or undergoing scatter as illustrated in figure 4.2.

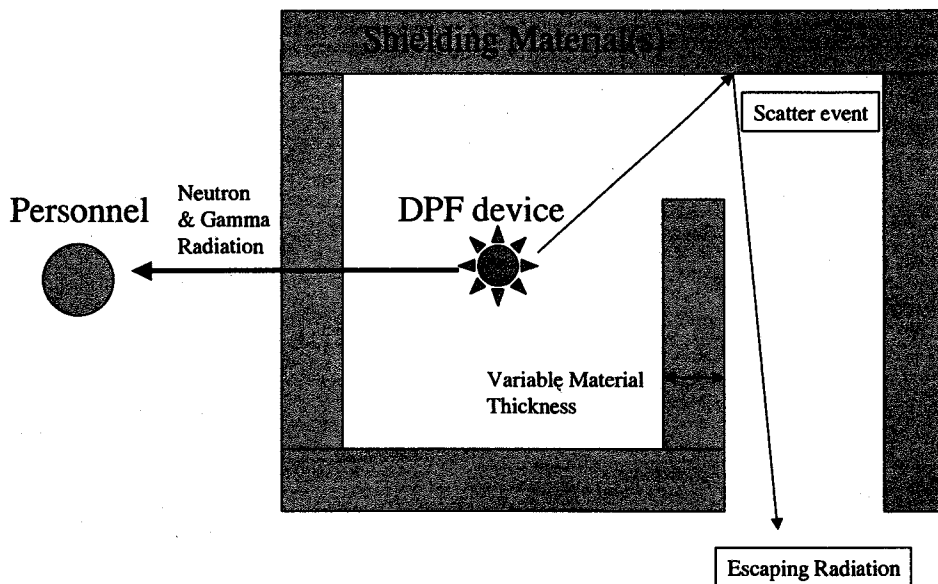


Figure 4.2 “Labyrinth” Shield Configuration and Possible Escape of Radiation

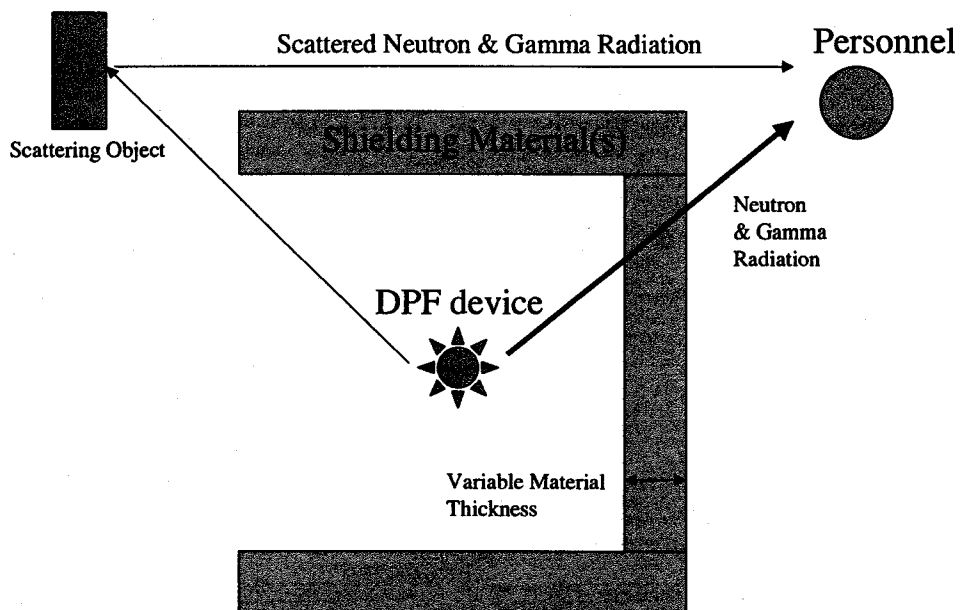


Figure 4.3 “Cave” Design with Direct LOS and Potential Scattered Radiation Hazard

Increasing LOS operation functionality is possible with a “cave” type design by removing one side of the square shield. This concept is shown in figure 4.3. LOS operation

is dramatically improved as experiments can be easily placed without interference from the shield. However, personnel in direct LOS with the device will not have the protection of any shielding. Additionally, scatter of the unshielded radiation off objects/walls could present a hazard to personnel on the shielded side as illustrated in figure 4.3.

The previous three options involve placement of shielding materials around the device on level flooring. An additional option is placement of the DPF device inside a concrete lined pit that already exists in the NTS building as illustrated in figure 4.4.

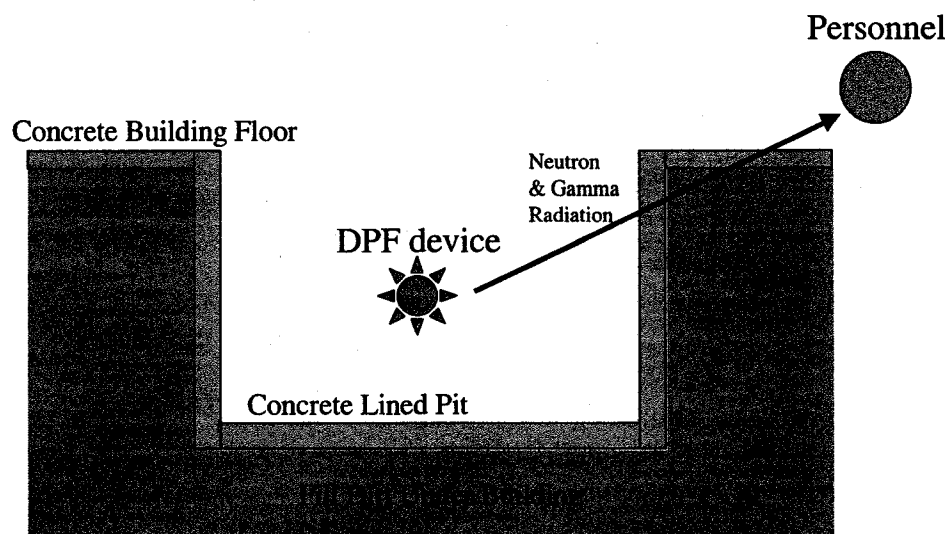


Figure 4.4 Existing Concrete Lined Pit Shield Concept

A major benefit of this shielding configuration is the ease of construction and reduced cost. The existing concrete lining along with the dirt fill under the building can be used as shielding. However a major downside is increased difficulty in LOS operation of the device as experiments must be suspended over the device or placed in the pit. Additionally, the device must be lifted from the pit for modifications, similar to the problems presented by the

square shield design of figure 4.1. Potential exposure to personnel exists from scattering radiation from the ceiling, similar to above ground configurations.

These shielding configurations were all examined with varying thicknesses and order of materials. Another modification that was examined included placement of lids composed of different materials overtop of the previous shielding configurations. Placing shielding material on top of the DPF device could reduce skyshine and exposure to personnel. Smaller shielding configurations placed directly around the DPF device in addition to the outer shields, while still allowing LOS operation, were also examined.

## CHAPTER 5

### RESULTS

#### 5.1 Comparison of Dose Calculation Methods

The primary goal of the current work was analysis of various shielding configurations in order to determine dose to personnel near the device. Before the calculation of dose, one must first determine the most effective dose calculation method. MCNPX can determine dose based on energy deposition of radiation in target materials, usually water or simulated human tissue. An alternate method is the use of direct flux-to-dose conversion factors where particle flux at a surface is determined and dose at that location is then a simple conversion factor.

The benefit of MCNPX calculated dose by energy deposition is accuracy. This method accounts for all particles that enter the phantom volume and all particles that exit. It is possible that radiation can enter a volume of material and leave while depositing little or no energy. MCNPX can account for this since only total energy deposited in a target volume is calculated. The downside of energy deposition methods is the amount of time required to run simulations and possible interference between target volumes. MCNPX can calculate flux more quickly using point detectors as opposed to tracking energy deposition. Interference between target volumes can occur if dose at multiple locations in close

proximity are desired as particles can scatter from one target volume to another.

Additionally, target volumes can shield each other if not arranged correctly.

Flux-to-dose conversion factors have the advantage of speed since point detectors can be used as opposed to tracking energy deposition in cells. A point detector in MCNPX is a location in space where flux is tallied without that detector causing any attenuation or disturbing the flux of radiation. Additionally, flux point detectors can never interfere with each other or shield other detectors. This offers the advantage of arranging flux detectors anywhere in the problem. The downside of using this method is the reliance on conversion factors. These conversion factors assume a uniform field of neutrons incident on a phantom. The flux-to-dose conversion factors examined in this work are from the NRC regulation 10CFR20 and are presented in table 5.1 with corresponding quality factors.

**Neutron Flux-to-Dose Conversion  
Factors:  
(NRC 10 CFR - 20.1004)**

MeV ranges	Q	(neutrons cm <sup>-2</sup> rem <sup>-1</sup> )
0 to 1E-3	2	9.80E+08
>1E-3 to 1E-2	2.5	1.01E+09
>1E-2 to 1E-1	7.5	1.70E+08
>1E-1 to 1	11	2.70E+07
>1 to 2.5	9	2.90E+07
>2.5 to 5	8	2.30E+07
>5 to 7	7	2.40E+07
>7 to 10	6.5	2.40E+07
>10 to 14	7.5	1.70E+07

Table 5.1 Neutron Flux-to-Dose Conversion Factors from NRC Regulations

The conversion factors in table 5.1 can be used to directly convert a neutron flux in neutrons/cm<sup>2</sup> to dose in rems. These conversion factors assume a uniform, monoenergetic

flux over a phantom of human tissue 30cm in diameter and 60cm high. To compare these values to MCNPX energy deposition methods, a phantom matching these specifications was modeled with a uniform monoenergetic neutron beam of varying energies. Figure 5.1 shows an MCNPX produced tally from the tracks of the primary neutrons on the tissue phantom.

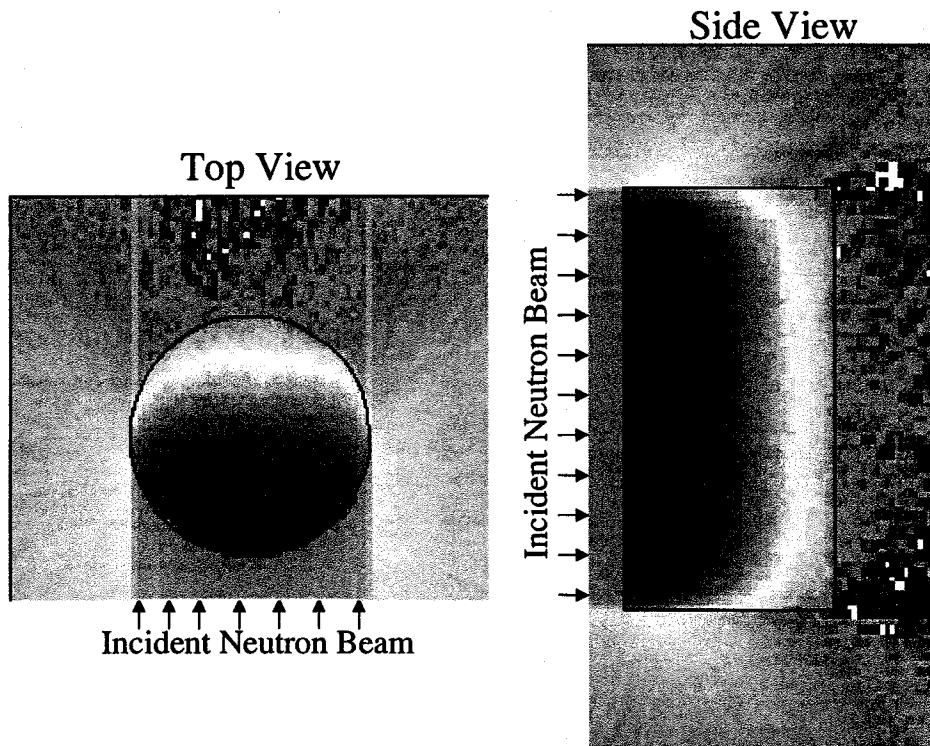


Figure 5.1 Cross-Sectional Views of Neutron Tracks through Phantom (MCNPX)

Using the geometry modeled in figure 5.1, which corresponds to the phantom described in 10CFR20, energy deposition in the phantom was calculated for the energies provided in table 5.1. The resulting MCNPX doses from energy deposition are presented in table 5.2. Energy deposition calculated in MCNPX is presented in MeV/gram after multiplication by the number of source particles to determine total energy deposited per gram in the target. The number of source particles over the frontal area of the phantom that would

produce 1 rem according to flux-to-dose conversion factors from table 5.1 were used as the number of source particles for energy deposition calculations in table 5.2. The incident neutron beam had an area of 30cm x 60cm (1800cm<sup>2</sup>) meaning that a flux resulting in 1 rem, as in the 60 MeV neutron case, of 16x10<sup>6</sup> n/cm<sup>2</sup> would require 2.88x10<sup>10</sup> neutrons to be used as a source.

Neutron Energy (MeV)	# Particles for 1 rem over 1800cm <sup>2</sup>	Resulting Dose from Radiation Types					Flux-to-Dose Overestimation Factor
		Neutrons (rems)	Electrons (rems)	Photons (rems)	Protons (rems)	Total Dose (rems)	
60	2.88E+10	0.5759	0.0024	0.0025	0.2250	0.81	1.24
40	2.52E+10	0.6105	0.0025	0.0026	0.0840	0.70	1.43
20	2.88E+10	0.6755	0.0040	0.0043	0.0112	0.69	1.44
14	3.06E+10	0.5783	0.0045	0.0048	0.0032	0.59	1.69
10	4.32E+10	0.6241	0.0056	0.0059	-	0.64	1.57
7	4.32E+10	0.5650	0.0031	0.0032	-	0.57	1.75
5	4.14E+10	0.4799	0.0028	0.0043	-	0.49	2.05
2.5	5.22E+10	0.3842	0.0042	0.0043	-	0.39	2.55
1	4.86E+10	0.1606	0.0031	0.0031	-	0.17	5.99
0.5	7.02E+10	0.1290	0.0051	0.0052	-	0.14	7.18
0.1	3.06E+11	0.0829	0.0187	0.0191	-	0.12	8.28

Table 5.2 Dose Calculation in Phantom for Energy Deposition in MCNPX

One can see from table 5.2 the total dose computed in the tissue phantom for a neutron beam of various energies. Dose was calculated for neutrons, electrons, photons and protons in order to account for secondary and scattered radiation created in the phantom. These doses were calculated using the same flux that would provide 1 rem using flux-to-dose conversions, as seen in column 2 of table 5.2. It is apparent that energy deposition in MCNPX calculates a smaller dose than the flux-to-dose conversion method. The overestimation of the flux-to-dose method is presented in the last column of table 5.2. One

can see that at higher incident neutron energies, better agreement exists between the two methods.

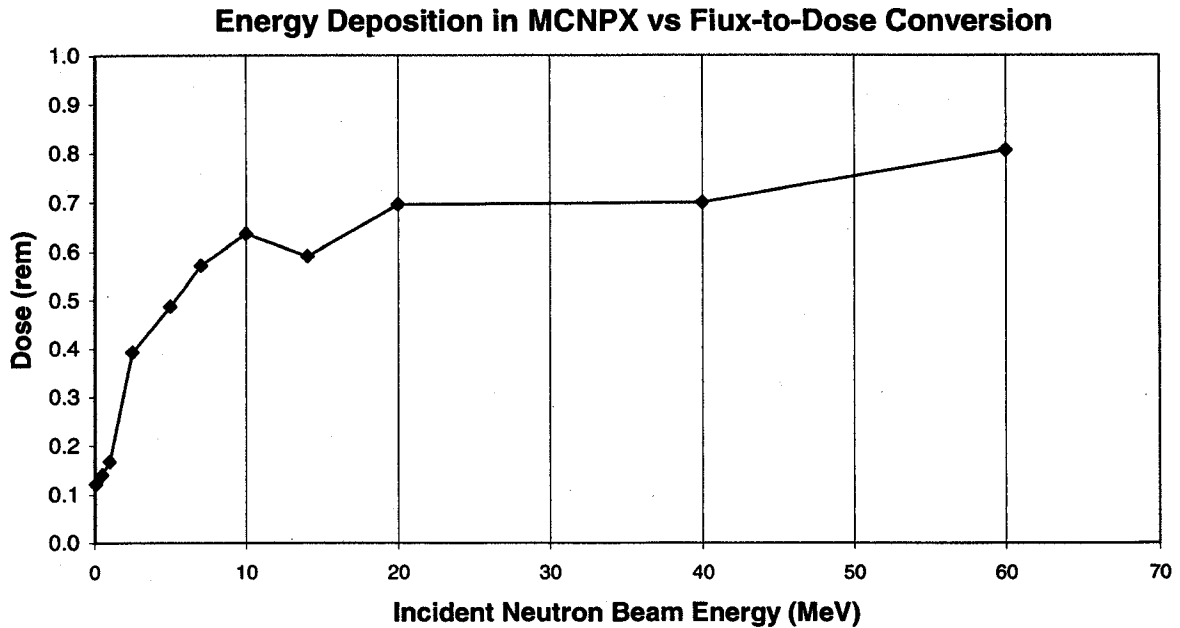


Figure 5.2 Comparison of MCNPX Energy Deposition Method to Flux-to-Dose Conversion

The improved agreement at higher energies can be seen in figure 5.2 with dose in the tissue phantom calculated from energy deposition versus energy of the incident neutron beam. By comparison, using flux-to-dose methods would have resulted in a calculation of 1 rem for all neutron energies in figure 5.2. A possible reason for this overestimation of dose is the escape of scattered neutrons as can be seen in figure 5.1. MCNPX can account for the escape of radiation that does not deposit all of its energy thus leading to a smaller dose calculation than simple flux-to-dose conversions. One can see that dose-to-flux conversions are very conservative in dose estimation and are therefore safe for use in shielding applications. However the larger overestimations of dose, over 8 times for lower neutron

energies, results in more shielding than necessary. In the current work, the primary neutrons will be 14 MeV and 2.45 MeV in addition to neutrons that are downscattered to low energies. Therefore, using flux-to-dose methods should result in an overestimation of dose by at least 1.69 times.

Quantifying the contribution of each radiation type to total dose is important when doing several dose calculations for different configurations. If possible, we can eliminate the tallying of a radiation type if the contribution is small enough and save computing time. From table 5.2, one can see that dose contribution from secondary radiation is very small for the incident neutron energies that we are concerned with, 2.45 MeV and 14 MeV. Lower incident neutron energies in the 0.1 MeV range have larger electron and photon dose contributions, over 15% each. However, as will be shown subsequently in the neutron flux spectrum of figure 5.5, the number of low energy neutrons that downscatter and reach the targets are much lower than the number of primary 14 MeV neutrons. We can therefore neglect secondary electron and photon dose contributions when compared to neutron dose for both the 2.45 MeV D-D and 14 MeV D-T reactions.

Protons, carrying a positive charge and a mass close to the neutron, have a quality factor of 10 for all energies and are therefore the most dangerous secondary radiation. However the protons do not contribute significantly to dose until about 20 MeV and above, outside the range we are concerned with. The tissue phantom is composed by weight of 10.2% hydrogen, 12.3% carbon, 3.5% nitrogen and 74% oxygen. A threshold exists for proton production in both carbon and oxygen, the dominant components of tissue, at 13.644 MeV and 10.246 MeV respectively. These thresholds can be seen on the proton production cross-section plot of figure 5.3. This means that neutrons with energy less than those

thresholds will not produce protons. As one can see from table 5.3, even the 14 MeV neutrons from the D-T reaction will have dose dominated by neutrons.

Neutron Energy (MeV)	Percent Dose Contribution			
	Neutron	Electron	Photon	Proton
60	71.46%	0.30%	0.32%	27.92%
40	87.26%	0.35%	0.37%	12.01%
20	97.20%	0.58%	0.61%	1.61%
14	97.89%	0.76%	0.81%	0.54%
10	98.19%	0.88%	0.93%	-
7	98.90%	0.54%	0.56%	-
5	98.55%	0.57%	0.89%	-
2.5	97.83%	1.08%	1.10%	-
1	96.27%	1.85%	1.88%	-
0.5	92.64%	3.65%	3.71%	-
0.1	68.65%	15.50%	15.85%	-

Table 5.3 Dose Contribution in Tissue from Radiation Types

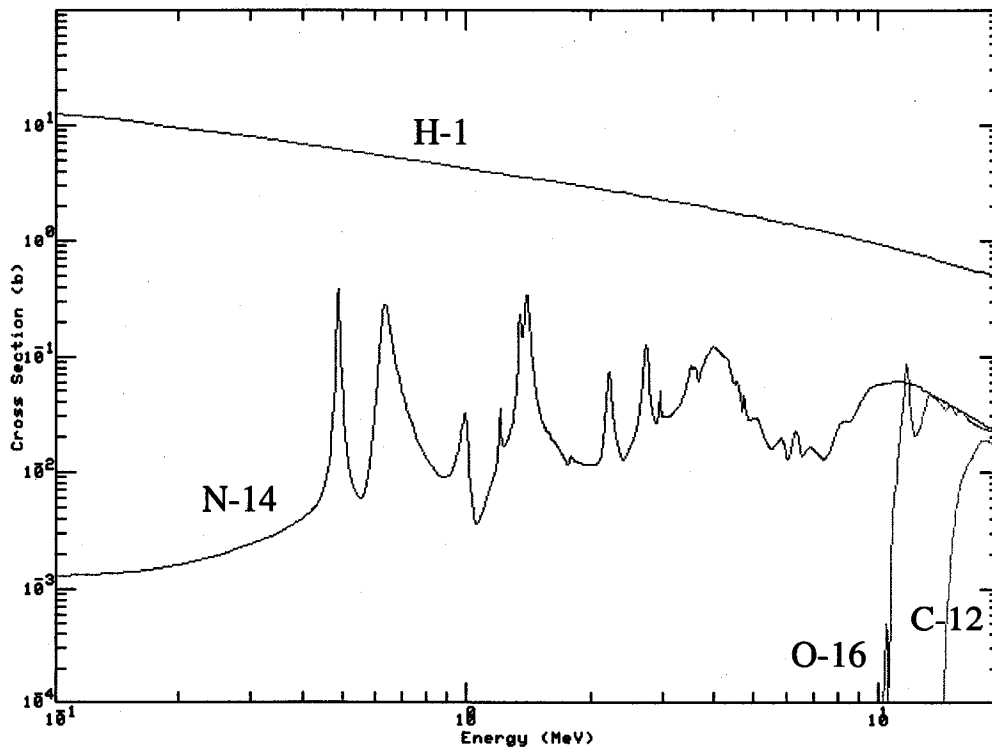


Figure 5.3 Proton Production Cross-Sections in Barns by Neutron Capture for N-14, C-12 and O-16. Hydrogen (H-1) Elastic Scattering Provided for Reference.

Based on the fact that 14 MeV neutrons and below have negligible dose contribution from protons, we can neglect this secondary radiation type along with the electrons and photons in further dose calculations. This allows us to save computing time as secondary particle tracking consumes large amounts of processing time.

Both the flux-to-dose conversion and energy deposition methods were compared using actual problem geometry to see if the predicted dose overestimation for 14 MeV incident neutrons occurs. These simulations used the source as an unshielded point source of 14 MeV neutrons in the new 11-102 building where the DPF device will be relocated with a tally point inside a steel trailer near the building. The first simulation used a point detector that simply measures flux at a position while the second used the same tissue phantom from previous calculations as shown in figure 5.4.

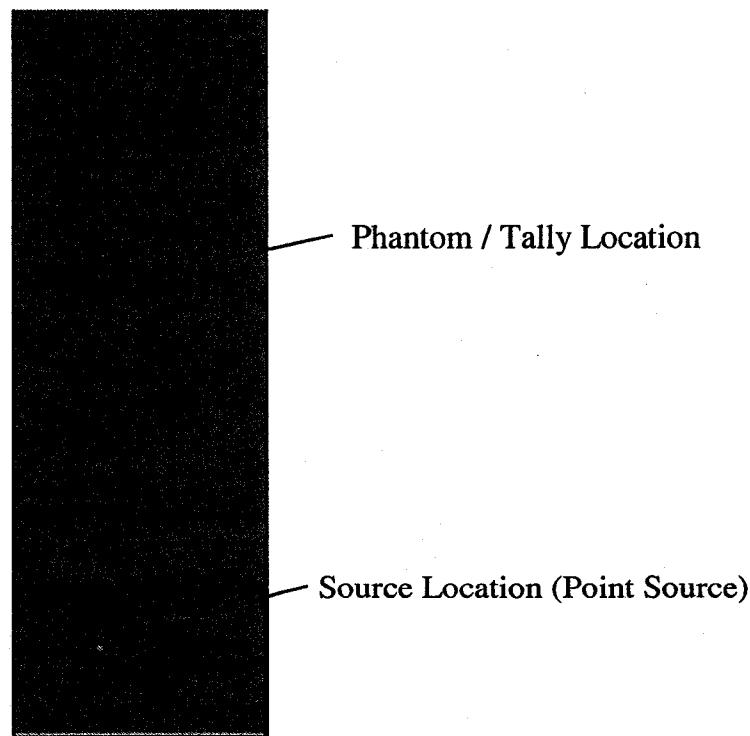


Figure 5.4 Source and Tally Locations for Dose Method Comparison (MCNPX)

The dose results of the point detector flux tally are presented in table 5.4 using the corresponding 10CFR20 dose conversion factors presented earlier in table 5.1. The second simulation utilized the tissue phantom and energy deposited in the phantom from neutrons and was then converted to dose using the quality factors. In addition to dose for both methods, computational time is also presented in table 5.4.

	Point Detector (Flux-to-Dose)	Tissue Phantom (Energy Deposition)
Dose (mrem)	8.27	3.80
Error (+/- mrem)	0.08	0.20
Runtime (min)	7.46	64.56

Table 5.4 Dose at Tally Location in Figure 13 Using Two Different Methods

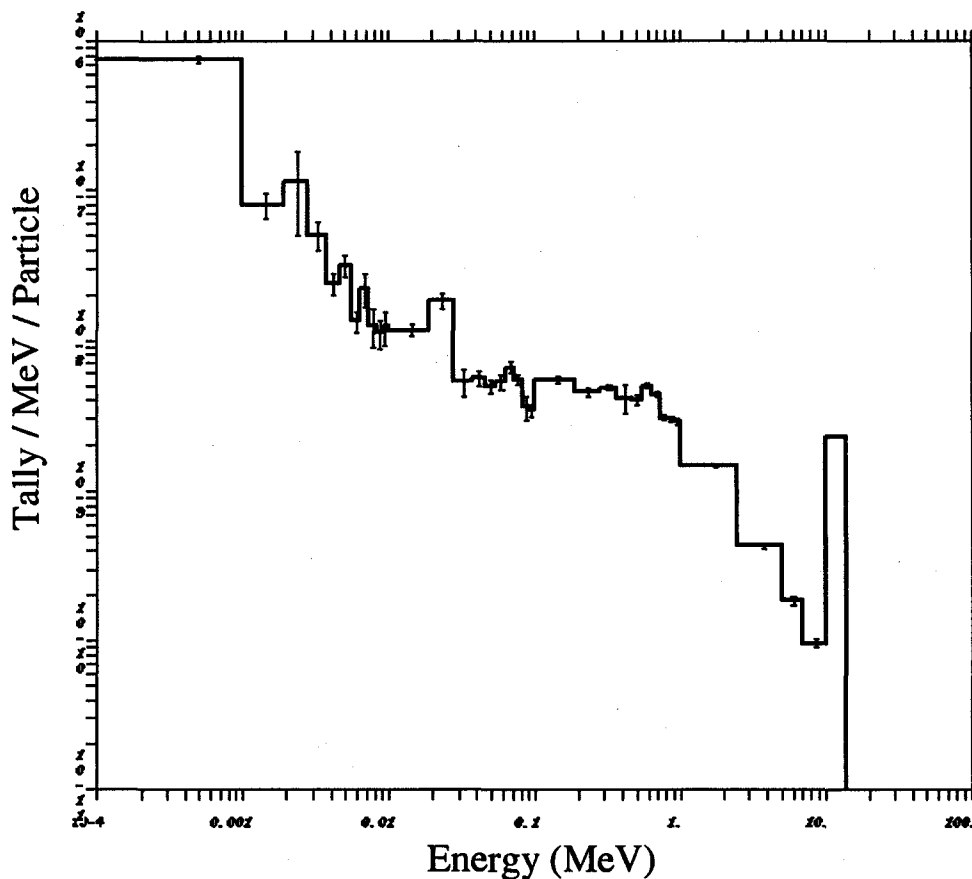


Figure 5.5 Neutron Flux Spectrum at Tally Point per Source Particle

One can see from table 5.4 that the flux-to-dose conversion method calculates dose to be about 2.2 times higher than the energy deposition method. This is in agreement with the dose overestimation factors of table 5.2 since some of the primary 14 MeV neutrons are downscattered as seen in the figure 5.5 spectrum. Note that figure 5.5 is flux per source particle emitted from the DPF device divided by the bin widths in MeV.

It is apparent that using a point detector for flux-to-dose conversion is much faster than energy deposition in a phantom, a little more than seven minutes compared to over an hour. Additionally, the benefits listed previously such as no self-shielding between point detectors can be useful. However the flux-to-dose method overestimates dose by 2.2 times in this case. The scientists at Bechtel Nevada have accepted this overestimation of dose since their health physics department uses these conversions in standard practice. The overestimation of dose is a convenient safety factor that will be implicit in all subsequent calculations. Due to the speed-up benefit, the accepted practice of using these conversion factors and the automatic safety factor, all final shielding designs in this work used flux-to-dose conversion factors rather than energy deposition methods.

Another benefit of using MCNPX is the accurate representation of scattered radiation that cannot be done by hand. The  $1/r^2$  relation of equation 3.11 is oftentimes used to estimate flux at a certain distance  $r$  from the source. However this only applies in a vacuum without objects nearby from which radiation could scatter. A comparison between the  $1/r^2$  relation and MCNPX results is presented here for the same geometry illustrated in figure 5.4. A flux tally was taken in the building at 10 ft and 20 ft from the radiation source and compared to the  $1/r^2$  approximation.

	Flux (n/cm <sup>2</sup> )	
	10ft Away	20ft Away
MCNPX	14.3E+06	5.77E+06
1/r <sup>2</sup> approx	8.57E+06	2.14E+06

Table 5.5 Comparison of Flux Calculated by MCNPX and 1/r<sup>2</sup>

One can see from table 5.5 that the actual flux is much greater than equation 3.11 would predict, 14.3E6 n/cm<sup>2</sup> as opposed to 8.57E6 n/cm<sup>2</sup>. Also, instead of falling off by 4 times at twice the distance, as the 1/r<sup>2</sup> relation predicts, the MCNPX results show that flux falls off by only 2.5 times. The scatter from the floor and walls almost doubles the flux at the tally point compared to primary radiation. This illustrates the importance of Monte Carlo methods in shielding calculations.

## 5.2 Square Shield Results

The simple square shield concept illustrated previously in figure 4.1 is presented first as a benchmark for other shields. The square shield provides excellent protection since radiation must pass directly through the barrier to reach personnel with no scattering routes aside from traveling up and out of the shield. Additionally, utilization of different shielding materials and configurations are examined here. For the square shield, the tally points are shown in figure 5.6 along with the shield location.

In the following shielding configuration and dose studies, it was assumed that the device was operating in the D-T configuration and producing 10<sup>13</sup> neutron pulses at 14 MeV. This assumes a worse case scenario since the D-D configuration produces only 10<sup>11</sup> neutrons of 2.45 MeV. Future analyses should include an evaluation of the 2.45 MeV D-D neutron dose for completeness.

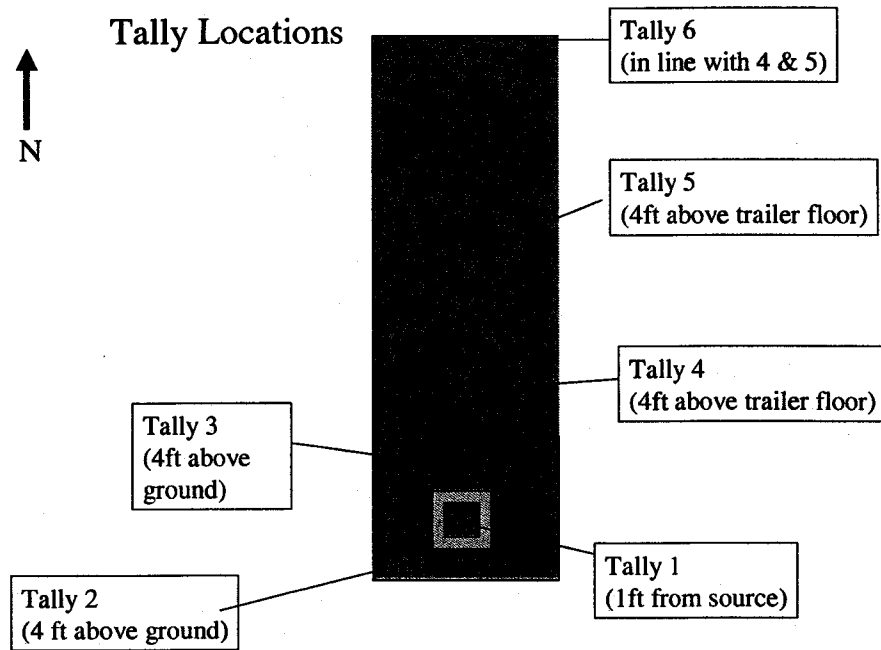


Figure 5.6 Tally Locations for Square Shield Designs

A cross-section of the square shield is shown in figure 5.7 with the source completely enclosed on four sides with 36in concrete shielding. The top is covered by a 12 in concrete slab underneath a 12 in borated polyethylene slab. The slabs must have a gap large enough to accommodate the multiple cables leading to the DPF device and so a “labyrinth” type of duct is provided to force multiple scattering of radiation exiting through the gap. At this point, the slabs are simply suspended in MCNPX. A final design on the chosen shield type includes steel supports. A mesh tally showing the effect of the labyrinth duct system is illustrated in figure 5.8. A mesh tally in MCNPX is a tally of particles consisting of a grid pattern with the number of particles passing through each element of the grid quantified by a color. In the right image of figure 5.8, red colors indicate the highest number of tracks while blue represents the least and white are grid points with zero neutron tracks.

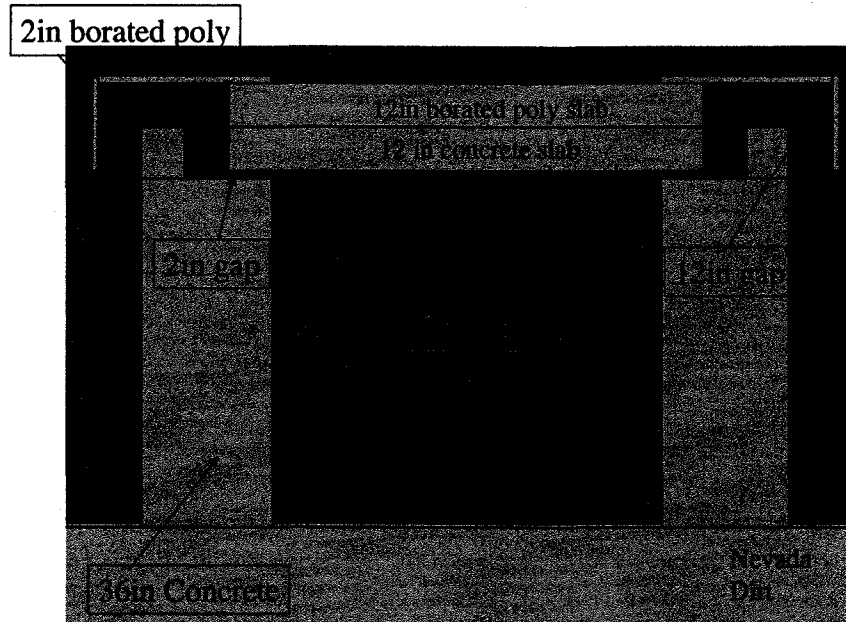


Figure 5.7 MCNPX Image of Square Shield with Top

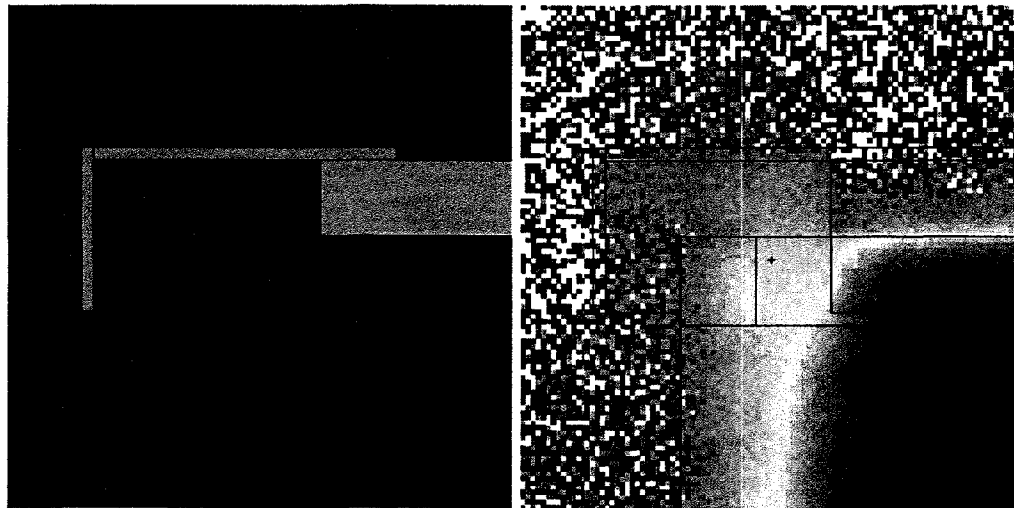


Figure 5.8 Duct System Showing Materials (left) and Mesh Tally of Neutron Flux (right)

The borated polyethylene was used due to its large weight percentage of hydrogen. As discussed earlier, light elements such as hydrogen are excellent neutron shielding material due to the large amount of energy lost in each collision of up to half of the neutron energy.

Composition of the polyethylene used in this study was, by weight, 13.65% hydrogen, 81.35% oxygen and 5% boron. The polyethylene is doped with boron since the natural isotopes of boron, B-10 and B-11, have increasing capture cross-sections for lower neutron energies as shown previously in figure 3.5. Use of the polyethylene to downscatter neutrons and boron to capture those lower energy neutrons greatly enhances the effectiveness of concrete, which contains only 1% by weight of hydrogen as shown in table 5.6.

<b>COMPOSITION:</b>	
<b>Atomic number</b>	<b>Fraction by weight</b>
1	0.010000
6	0.001000
8	0.529107
11	0.016000
12	0.002000
13	0.033872
14	0.337021
19	0.013000
20	0.044000
26	0.014000

Table 5.6 Composition of "Portland" Concrete used in this Study with density of 2.3 g/cm<sup>3</sup>

<b>Location</b>	<b>Neutron Dose</b>	
	<b>(mrem/shot)</b>	<b>(+/- error)</b>
1	51928	5
2	0.743	0.0022
3	0.586	0.0015
4	0.138	0.0006
5	0.020	0.0003
6	0.004	0.0000

Table 5.7 Doses at Six Tally Locations for Square Shield with Top from a 10<sup>13</sup> Yield of 14 MeV Neutrons

Dose results from shielding the device with this configuration are presented in table 5.7 for the six tally points of interest. Note that most personnel will be in the trailer at locations 4 or 5 during the testing and that the 100 mrem per year is the limit set by Bechtel Nevada. From table 5.7, one can see that personnel in the trailer at point 4 will receive 100 mrem after about 720 shots of the device. This means the device could be fired 720 times over the course of 1 year while personnel remain below the 100 mrem/year dose limit. For the purpose of this study, the effectiveness of each shielding type was rated by the number of times the device can be fired before personnel receive 100 mrem at tally point 4. The other tally points will be monitored, but it is unlikely that personnel will be in the building (points 2 or 3) during firing. Tally point 1 is provided as a reference only 1 foot from the device since personnel will be restricted from this area due to the immense dose from each shot.

For the next square shield configuration, we attempt to further reduce dose by adding additional materials to the shielding. Borated paraffin is paraffin doped with boron, 14.12% hydrogen, 80.88% oxygen and 5% boron by weight, properties very similar to polyethylene. The borated paraffin was added outside the concrete shield using 4 in thickness with a 2 in borated poly “floor” added inside the device to reduce neutron scatter from the ground and provide absorption as shown in figure 5.9.

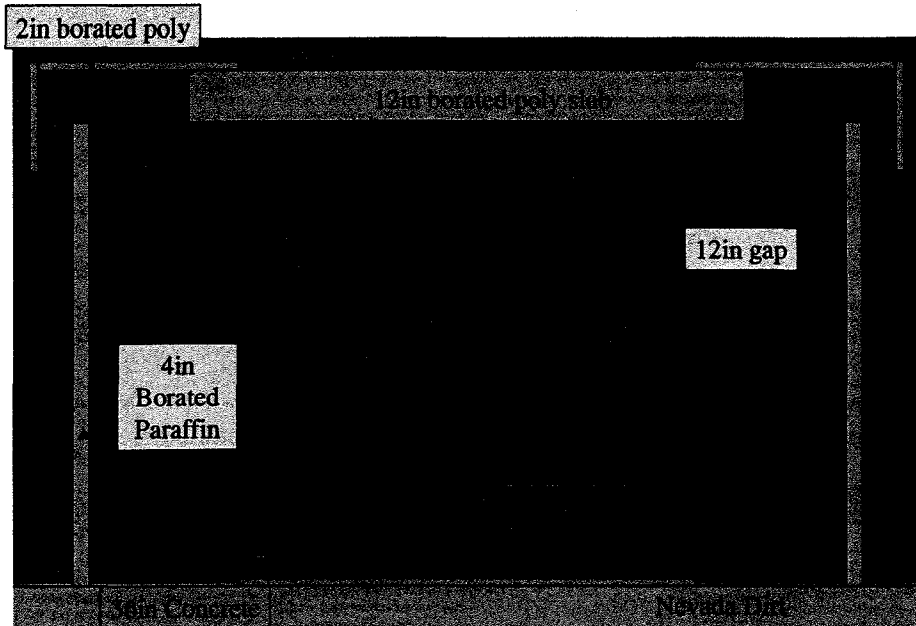


Figure 5.9 Square Shield with Additional Shielding Materials

Location	Neutron Dose	
	(mrem/shot)	(+/- error)
1	51693	5
2	0.347	0.0018
3	0.316	0.0014
4	0.085	0.0006
5	0.012	0.0002
6	0.003	0.0000

Table 5.8 Doses For Square Shield with Additional Materials from a  $10^{13}$  Yield of 14 MeV Neutrons

From this simple addition of borated polyethylene to the floor and borated paraffin outside the concrete, we reduced the dose to point 4 in the trailer by almost 40% as shown in table 5.8 to 0.085 mrem per shot. The device could now be fired over 1100 times before reaching the 100 mrem limit at point 4.

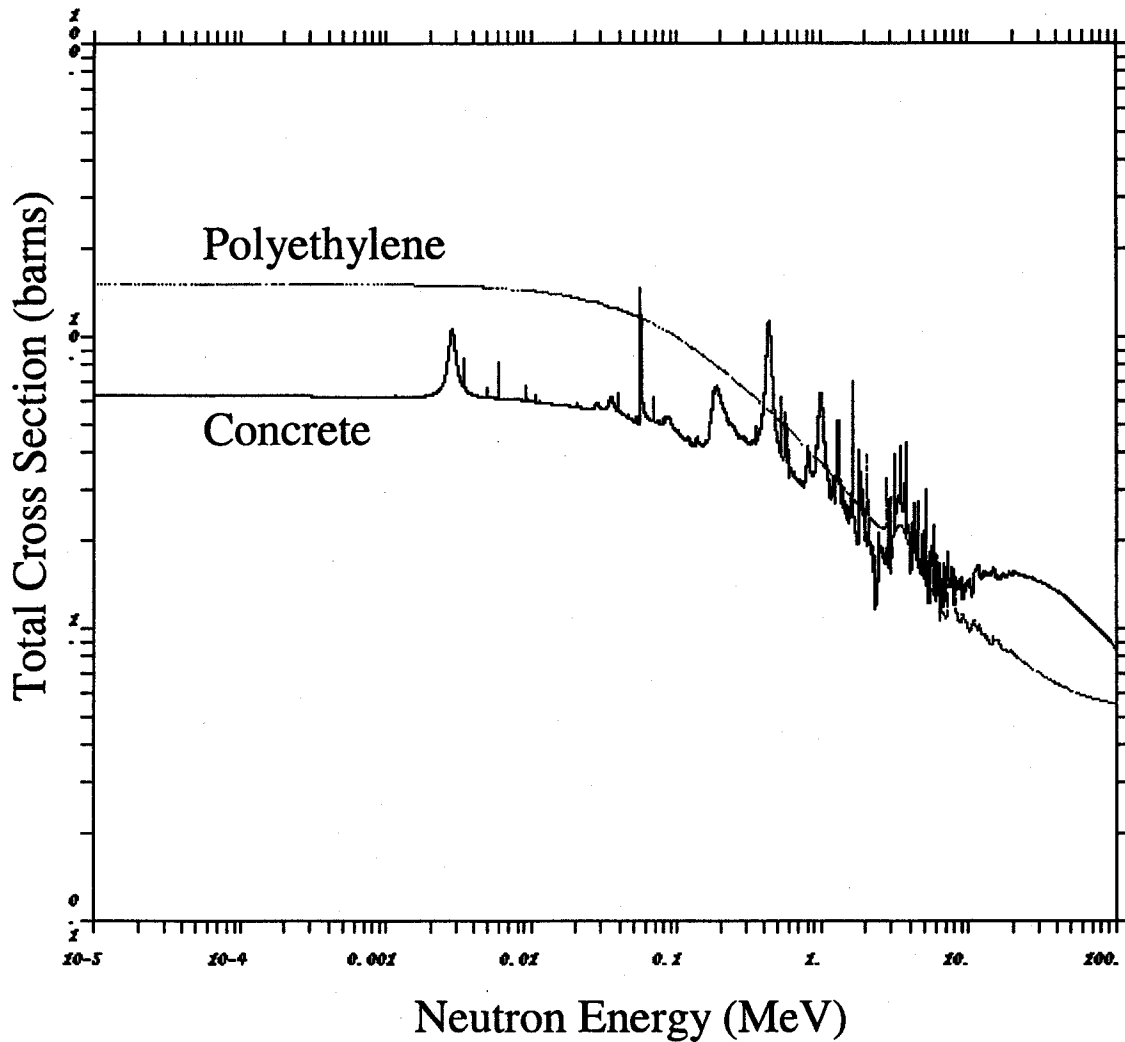


Figure 5.10 Total Neutron Cross Section for Polyethylene (non-borated) and Concrete

Adding additional polyethylene and paraffin to the shield made primarily of concrete greatly decreased dose. Total neutron cross-sections for polyethylene and concrete are presented in figure 5.10 for reference. The larger hydrogen content of the polyethylene creates a greater cross-section and thus better attenuation at neutron energies below about 4 MeV. One can see that layering concrete, which has a larger cross-section at higher neutron energies, in front of polyethylene will cause downscattering in the concrete first and then further downscattering in the polyethylene.

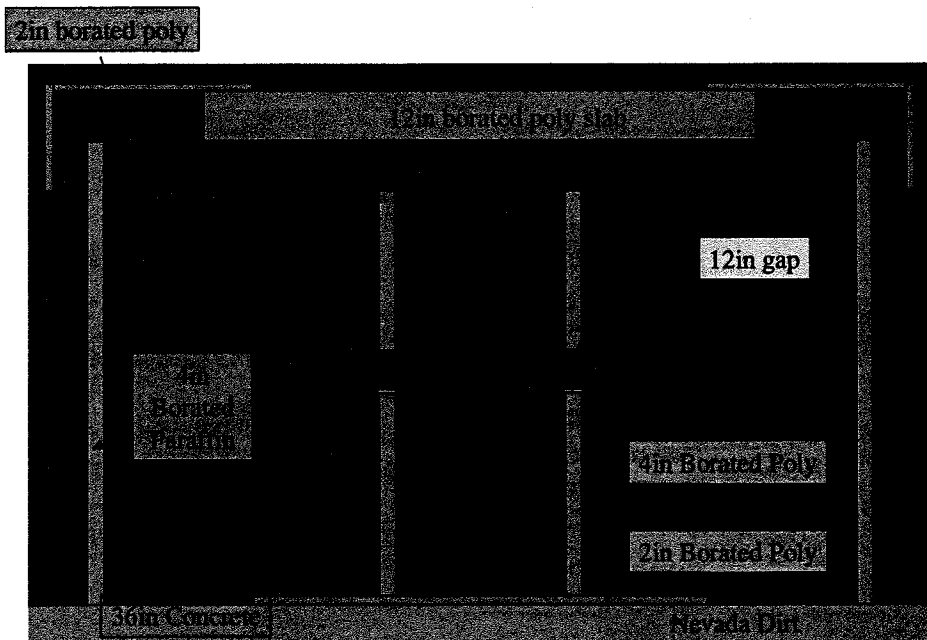


Figure 5.11 Square Shield With Additional Inner Shielding

Continuing with the addition of shielding material, we added 4 in of borated poly around the source inside the shield. The gap in the inner shielding provided in figure 5.11 would allow LOS to the device. This inner shielding further reduced dose at point 4 by almost 35% to 0.055 mrem per shot, as one can see in table 5.9. This inner shield combined with the previous addition of materials would allow over 1800 shots per year before reaching the 100 mrem limit.

Location	Neutron Dose	
	(mrem/shot)	(+/- error)
1	52616	5
2	0.225	0.0010
3	0.207	0.0012
4	0.055	0.0006
5	0.008	0.0002
6	0.002	0.0000

Table 5.9 Neutron Doses for Square Shield with Additional Inner Shielding from a  $10^{13}$  Yield of 14 MeV Neutrons

### 5.3 Labyrinth Results

While the square shield is effective at reducing dose, the usability of the device is severely limited since the roof of the shield must be removed whenever access to the device is required. Additionally, no direct LOS is available apart from the small area inside the shield near the device. The issue of access can be resolved by using a labyrinth concept, illustrated previously in figure 4.2. This configuration requires radiation to undergo scatter before leaving the shield while allowing easy access to the device. The layout for the labyrinth tally points is identical to the square shield as illustrated in figure 5.12.

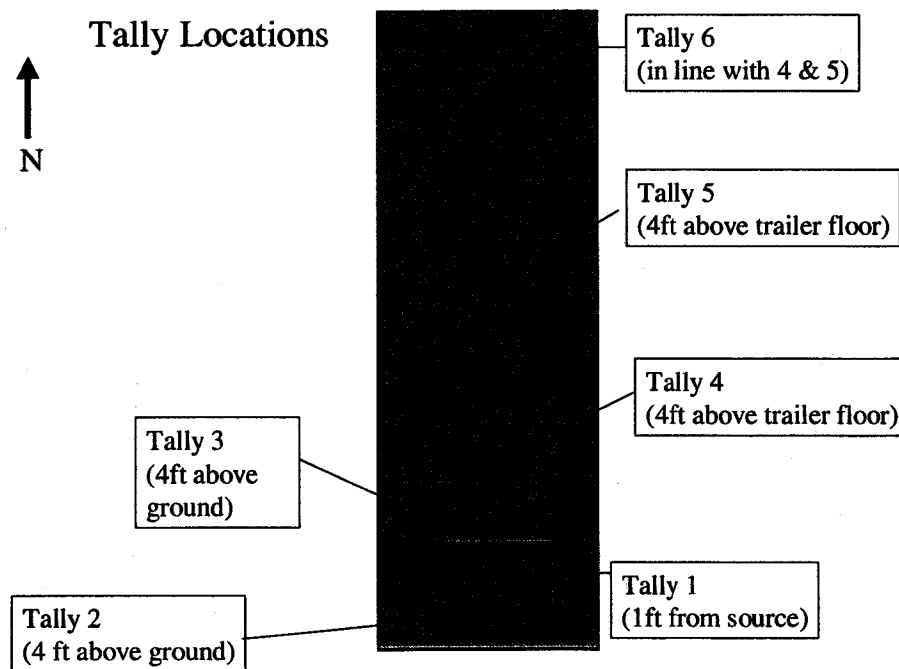


Figure 5.12 Tally Point Locations for Labyrinth Designs

### Labyrinth Top View

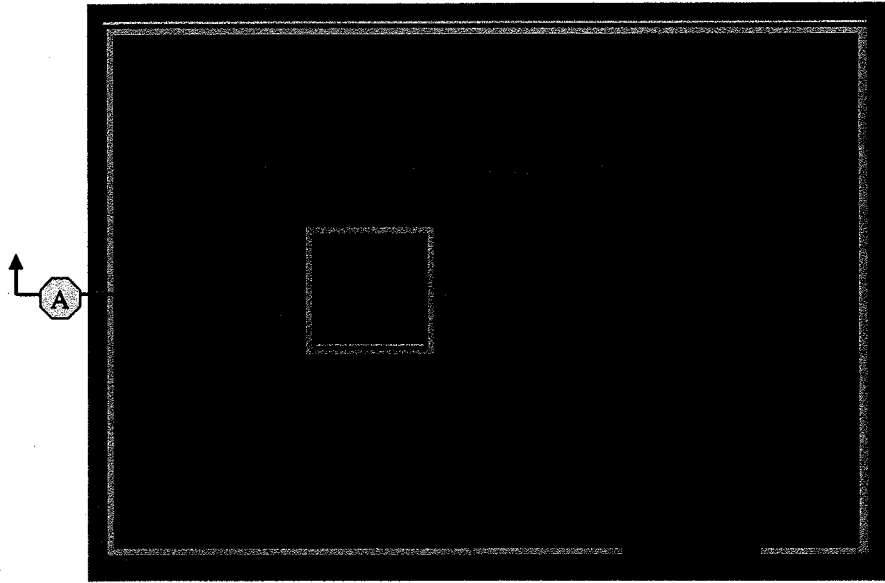


Figure 5.13 Top view of the “Labyrinth” Design

### Side View A

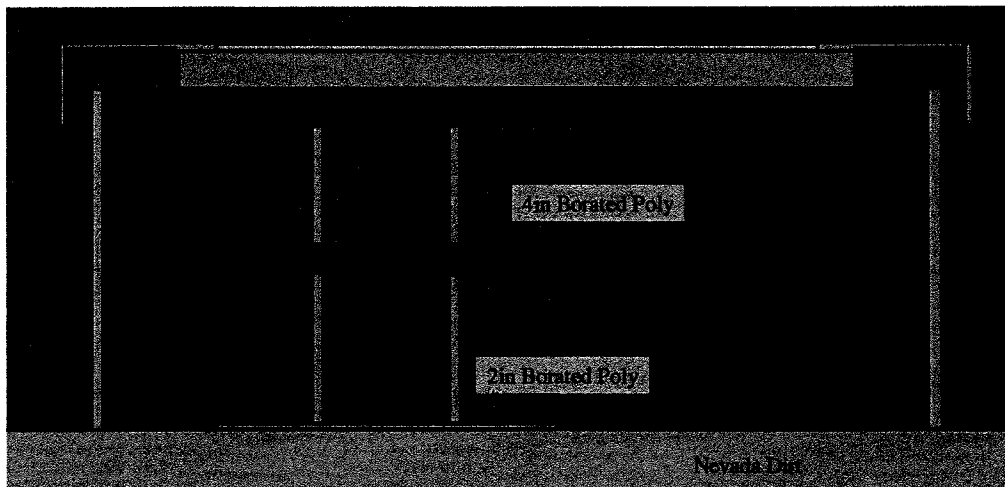


Figure 5.14 Cross-Sectional Side View of Labyrinth in Figure 23

The labyrinth of figures 5.13 and 5.14 uses the same additional shielding materials used previously in the square shield. A mesh tally of the labyrinth is presented in figure 5.15 to help illustrate the multiple scatter concept for radiation that escapes. The mesh tally quantifies neutron tracks. One can see that neutrons escape through the entrance by scattering.

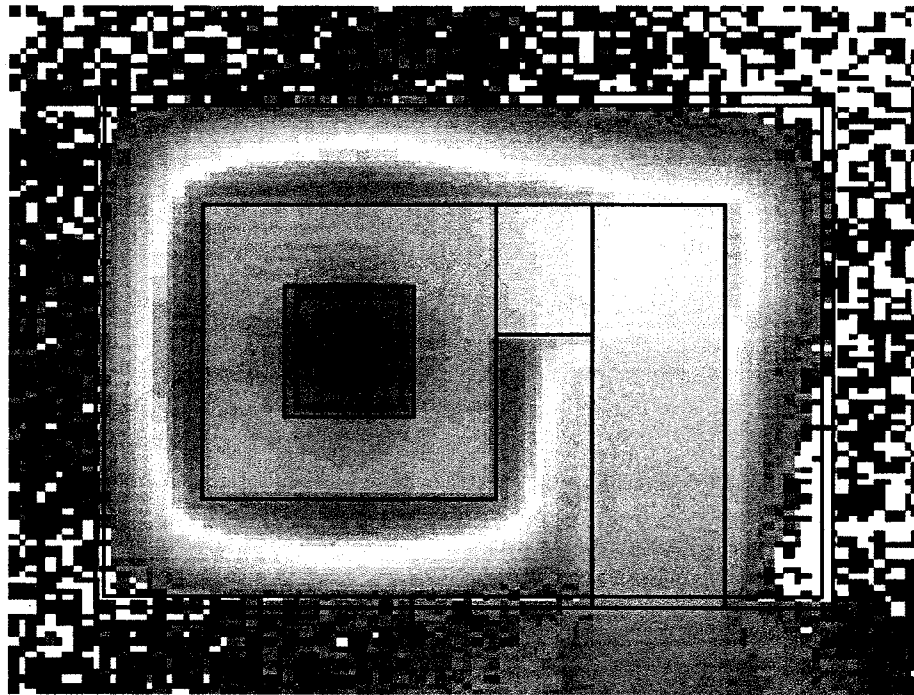


Figure 5.15 Mesh Tally of Neutron Tracks for the Labyrinth Concept

Location	Neutron Dose	
	(mrem/shot)	(+/- error)
1	52613	5
2	0.280	0.0020
3	0.204	0.0011
4	0.053	0.0004
5	0.008	0.0002
6	0.002	0.0000

Table 5.10 Neutron Doses for Labyrinth Shield from a  $10^{13}$  Yield of 14 MeV Neutrons

From table 5.10, we see that the dose to point 4 is very close and actually smaller than the dose when using the square shield, 0.053 mrem for the labyrinth as opposed to 0.055 mrem for the square shield. Despite the possibility of scattering escape by the neutrons as seen in the mesh tally of figure 5.15, the opening of the labyrinth points away from the tally points of concern and escaping neutrons must travel away from points 4, 5 and 6. Using the labyrinth in this configuration results in over 1880 shots per year being acceptable while providing much better access to the device than the square shield.

The added cost of borated poly and paraffin leads us to investigate the effect of removing the boron and using pure polyethylene and paraffin instead. Conventional shielding technique uses boron to capture thermal neutrons. However in our case the personnel are located so far from the device that thermalized neutrons are unlikely to reach them before interaction in the air. Additionally, non-borated poly and paraffin have slightly higher hydrogen weight percentages. Non-Borated poly is 14.37% hydrogen and non-borated paraffin is 14.86% hydrogen by weight.

Location	Neutron Dose	
	(mrem/shot)	(+/- error)
1	52674	5
2	0.299	0.0008
3	0.208	0.0007
4	0.051	0.0004
5	0.007	0.0001
6	0.002	0.0000

Table 5.11 Neutron Doses for Labyrinth Shield with Non-Borated Materials from a  $10^{13}$  Yield of 14 MeV Neutrons

This additional weight percentage of hydrogen, and since thermalized neutrons are unlikely to reach tally point 4, leads to the results in table 5.11 with the dose being slightly lower for non-borated poly and paraffin. Over 1950 shots per year can be done with this configuration while remaining below the 100 mrem limit. From these results, the borated poly and paraffin are unnecessary and non-borated materials could be used to save on cost.

Reducing the thickness of concrete would also save on cost of the shielding. Instead of 36in concrete, 18in concrete with the same poly and paraffin used previously is modeled. This 18in thick concrete shield as modeled in MCNPX is illustrated in figure 5.16 along with a cross-section in figure 5.17.

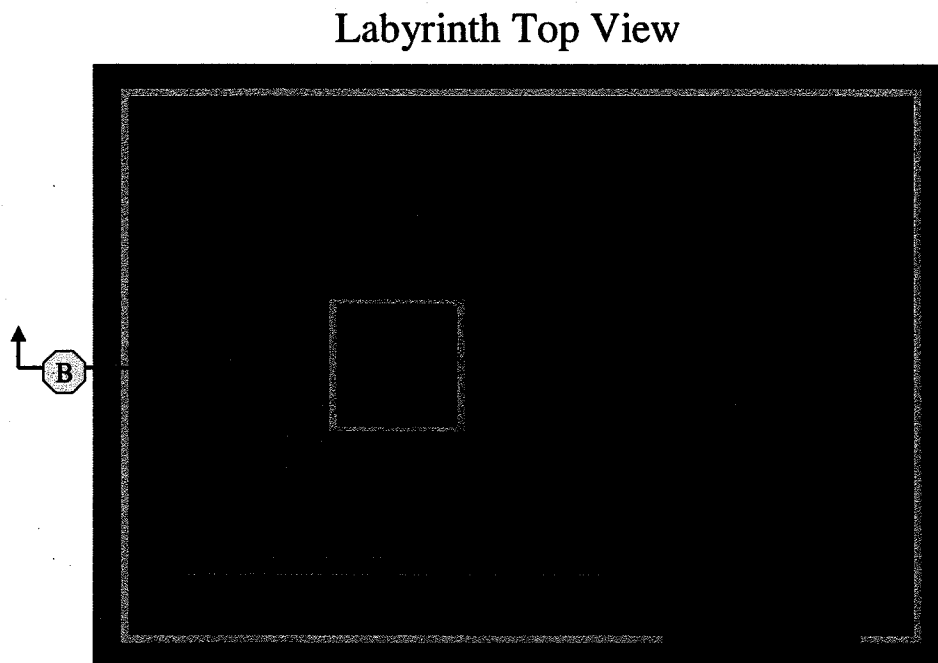


**Figure 5.16 Labyrinth Shield with 18in Concrete Shielding**

## Side View B

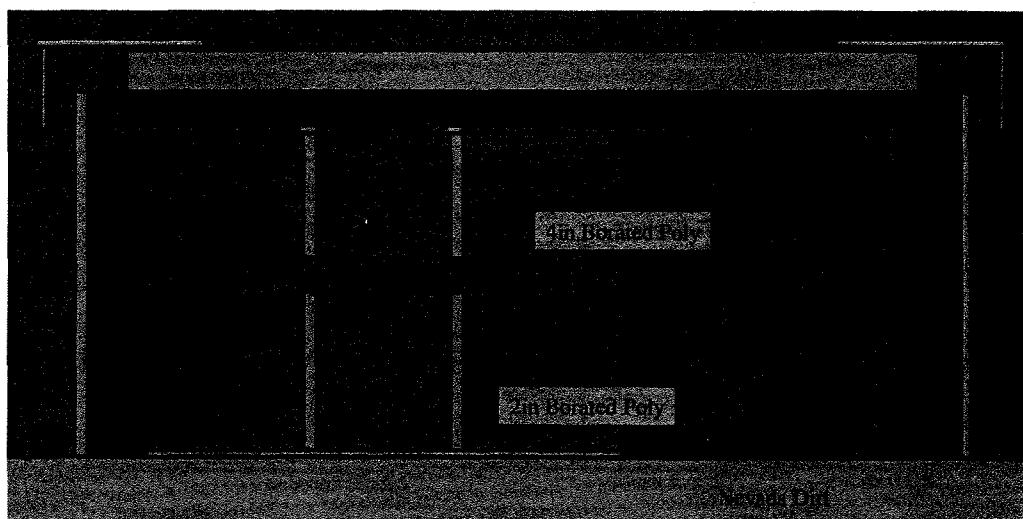


Figure 5.17 Cross-Sectional View of 18in Concrete Labyrinth Shielding

Location	Neutron Dose	
	(mrem/shot)	(+/- error)
1	52546	5
2	1.91	0.004
3	1.67	0.004
4	0.406	0.0014
5	0.065	0.0007
6	0.015	0.0001

Table 5.12 Neutron Doses with Thinner 18in Concrete Walls from a  $10^{13}$  Yield of 14 MeV Neutrons

One can see from table 5.12 that replacing the 36in concrete slabs with 18in material increased the dose significantly. The dose to tally point 4 in the trailer is now 0.406 mrem per shot, allowing about 240 shots per year compared to over 1950 shots per year with the 36in concrete. Clearly it is more effective to use the 36in concrete rather than 18in.

## 5.4 Cave Shield Results

A design that provides easy access to the device and LOS operation is the “cave” concept illustrated previously in figure 4.3. This shield is the most versatile design but also the least effective in radiation protection since one side of the shield is removed. For this shield, we removed one side of the square shield simulated previously so that the open side faces south and away from tally 4. This configuration is shown below in figures 5.18 and 5.19. The same 36in concrete thickness was used along with a concrete and poly top and outer and inner paraffin/poly.

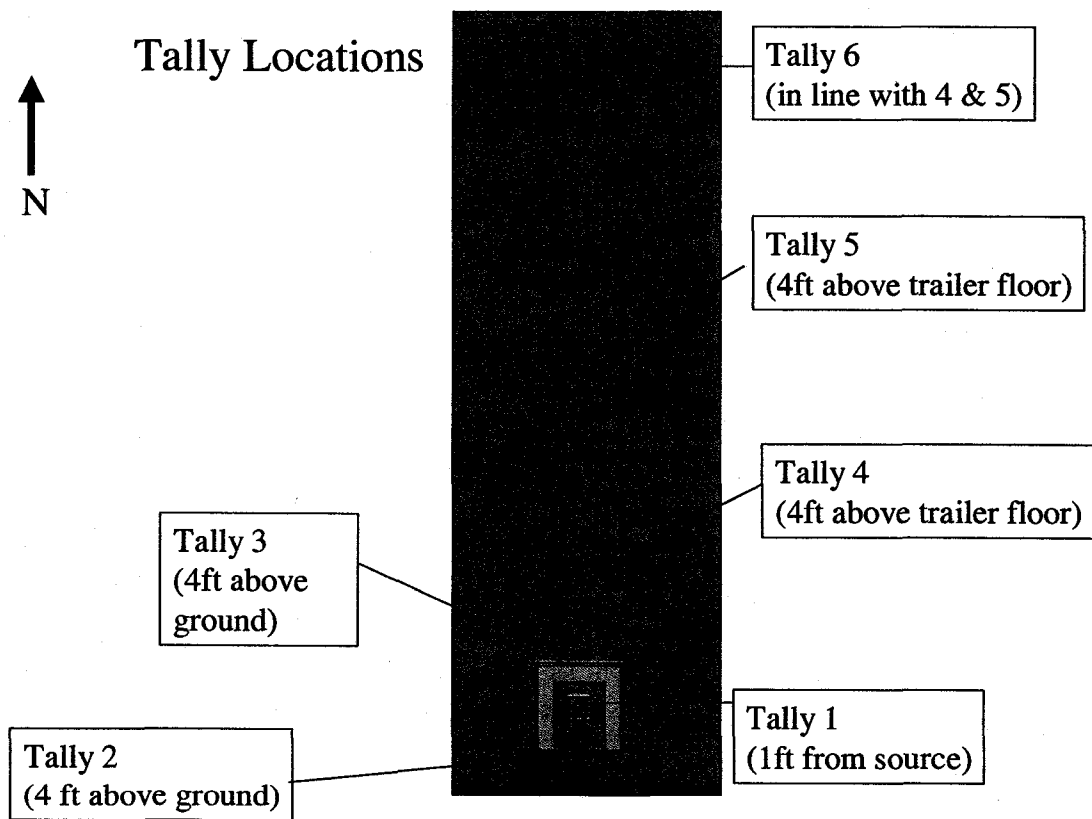


Figure 5.18 Tally Locations for “Cave” Shield

## Cave Top View

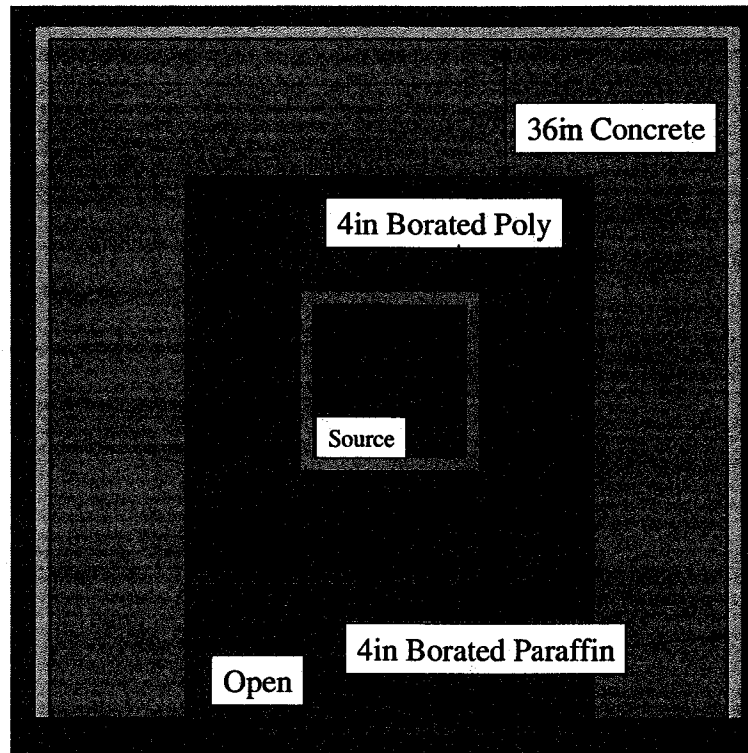


Figure 5.19 Top View of “Cave” Shield Showing Open Side

Location	Neutron Dose	
	(mrem/shot)	(+/- error)
1	52585	5
2	34.0	0.03
3	1.36	0.003
4	0.446	0.0013
5	0.077	0.0004
6	0.018	0.0001

Table 5.13 Neutron Doses with Cave Shield from a  $10^{13}$  Yield of 14 MeV Neutrons

One can see the dose at tally point 4 in the trailer was now significantly higher than either the 36in concrete labyrinth or the 36in square shield designs. A little over 220 shots

can be done per year before reaching the 100 mrem limit. Additionally, tally point 2 becomes hazardous to personnel inside the building due to its unshielded LOS to the device.

At this point, we also examined the effect that occurs from neutrons exiting the top of the shield and reflecting back to the ground by interaction with air and the ceiling of the building, sometimes called “skyshine”. The removal of the lid on the cave shield has a significant effect on dose to all the points as one can see below in table 5.14. Most notably, the dose to point 4 in the trailer is now 2.63 mrem per shot resulting in only 38 shots per year before reaching the 100 mrem limit. From these results it becomes apparent that a cover shield is required for all shield designs to provide adequate protection.

Location	Neutron Dose	
	(mrem/shot)	(+/- error)
1	52503	16
2	40.8	0.19
3	9.83	0.090
4	2.63	0.023
5	0.382	0.0100
6	0.080	0.0013

Table 5.14 Neutron Doses with Cave Shield and no Roof from a  $10^{13}$  Yield of 14 MeV Neutrons

### 5.5 Pit Shield Results

The existing concrete lined pit in the building provides an additional option for shielding. With a shielding top of concrete and poly in place, the pit shield can provide complete protection with minimal cost. This design can be seen as a compromise between versatility and protection since LOS operation is possible with a gap in the top shield to allow experiments at ground level or slightly elevated height to “see” the plasma focus point. The top shield must still be removed by crane to access the device, causing similar access and

maintenance problems as the square shield. At this point in the work with Bechtel Nevada, it was desired that additional tally points be added to the simulation. Tally points 2 through 6 were located in the same spot as previous calculations for comparison. Tally point 1 was now located 2.5 ft from the source, which had been relocated into the existing pit in the eastern side of the building as illustrated in figure 5.20. Points 8, 9 and 10 were added at an angle to the building and tally point 7 (not shown) was directly over the source outside the roof of the building.

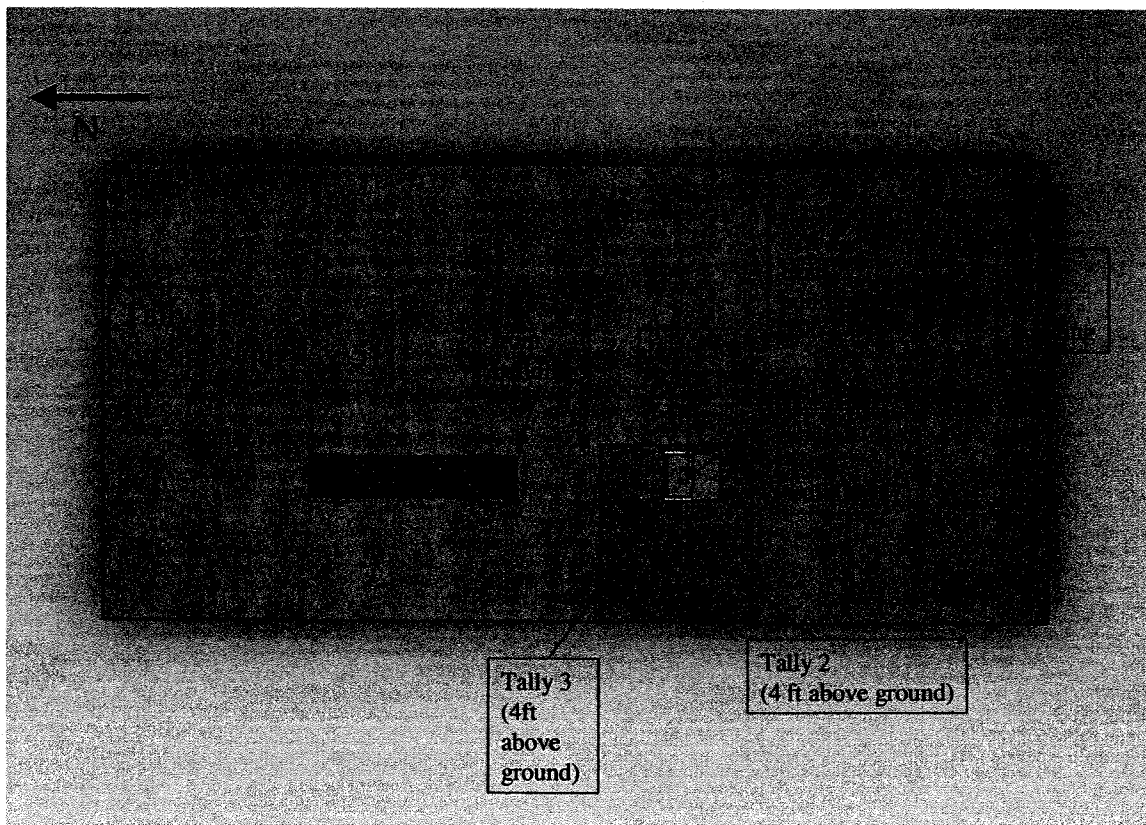


Figure 5.20 Tally Locations for Pit Shield Configuration

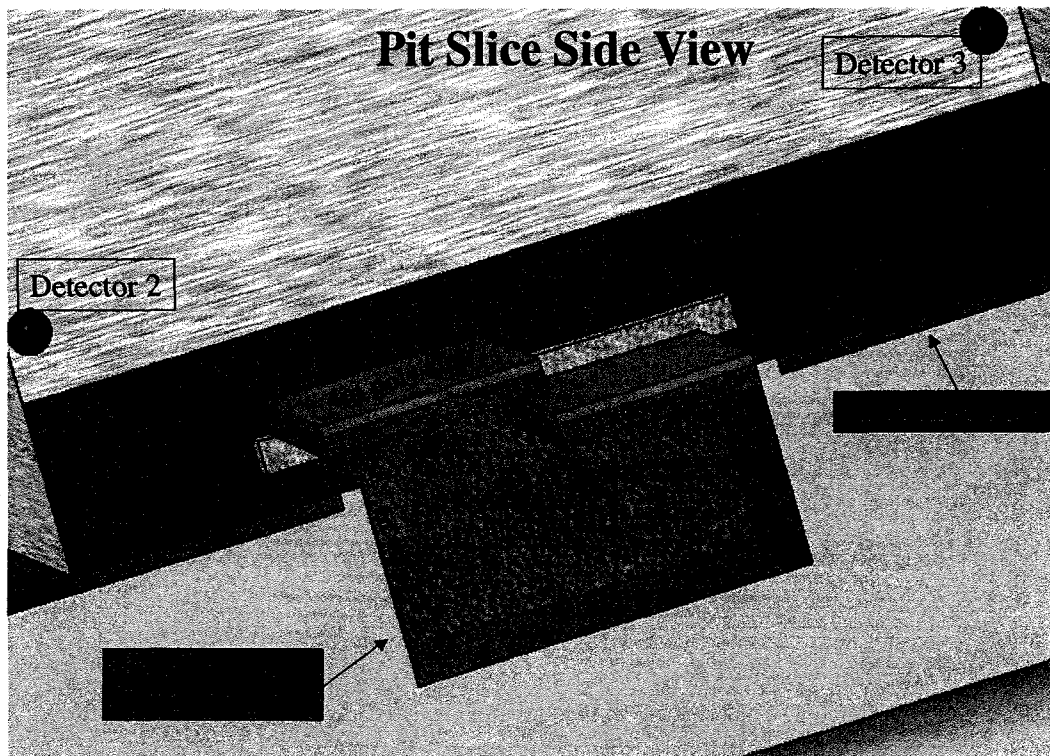


Figure 5.21 Side View of Pit Shield with Concrete and Poly Top

Location	Neutron Dose	
	(mrem/shot)	(+/- error)
1	9331	2
2	1.28	0.004
3	0.870	0.0028
4	0.581	0.0071
5	0.067	0.0049
6	0.011	0.0002
7	20.8	0.32
8	1.93	0.005
9	0.351	0.0038
10	0.117	0.0013

Table 5.15 Neutron Doses with Pit Shield from a  $10^{13}$  Yield of 14 MeV Neutrons

The first pit shield simulated used a 4in poly slab on top of an existing 8in concrete slab as a lid as shown in figure 5.21. This lid is already in two parts that allows a LOS gap

and to run cables to the DPF device. One can see from table 5.15 that dose to tally point 4 was 0.581 mrem per shot, over ten times higher than the 0.053 mrem per shot that can be obtained with the 36in concrete labyrinth. The pit shield concept is an inexpensive option since the pit and top are already in place and therefore needed further refinement to attempt to lower the dose.

To reduce dose with the pit shield, we added material to seal the gap created in the lid. The first option examined is the use of polyethylene blocks as illustrated in figure 5.22. The second option was the use of water filled steel boxes as illustrated in figure 5.23.

### Pit Slice Side View (MCNPX)

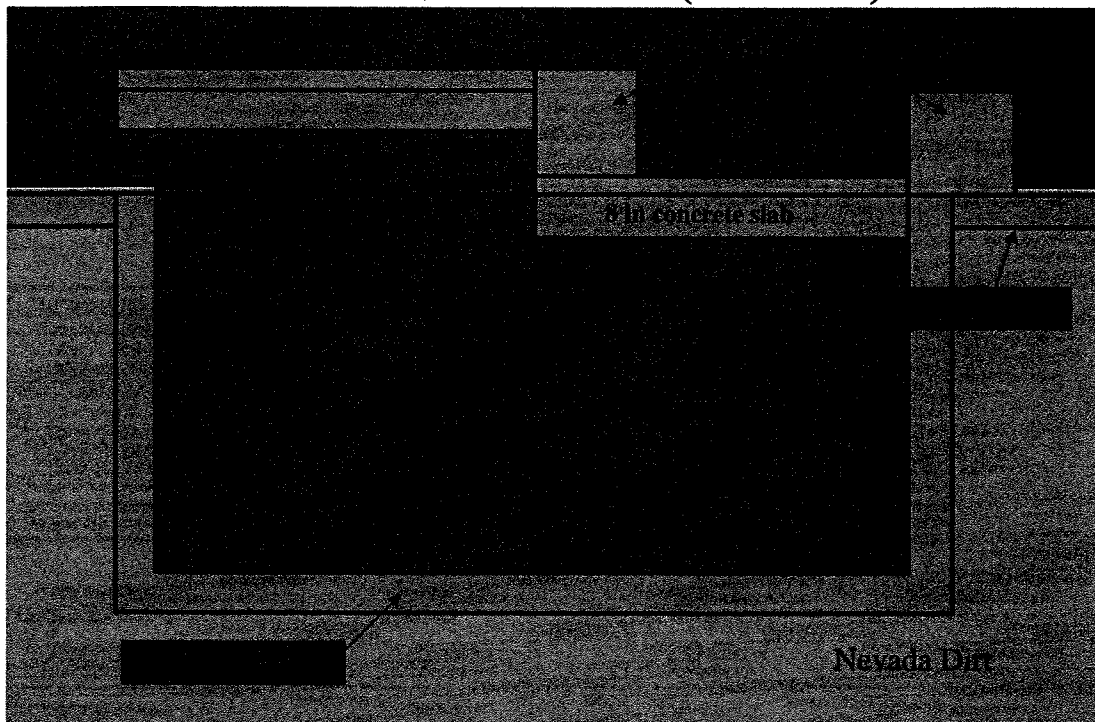


Figure 5.22 Pit Shield with Additional Polyethylene as a Gap Sealers

## Pit Slice Side View (MCNPX)

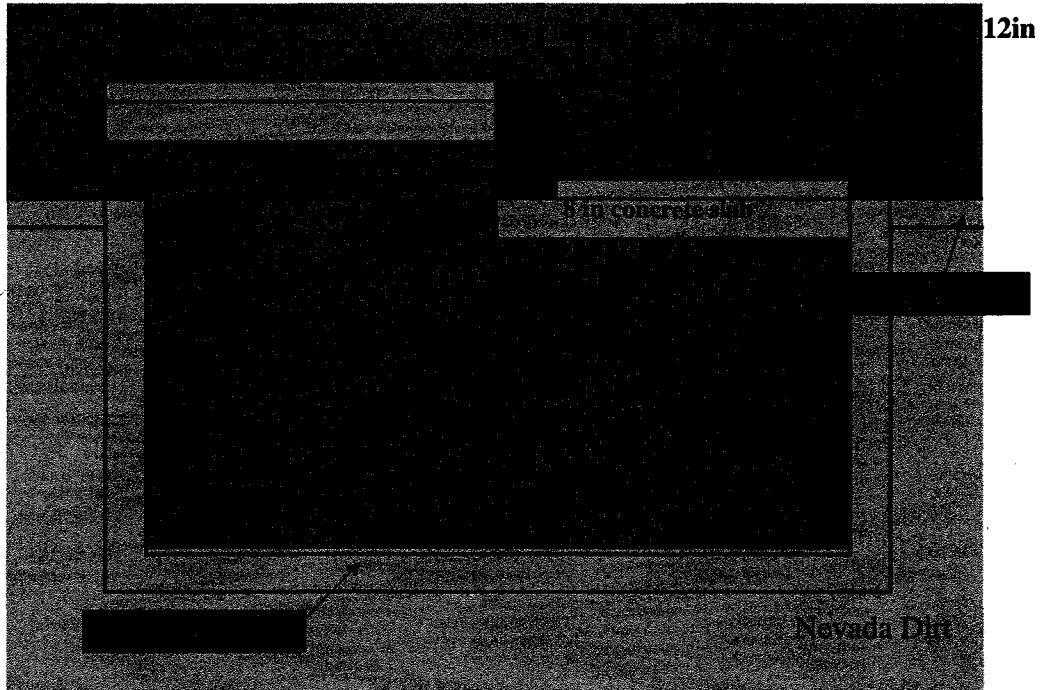


Figure 5.23 Pit Shield with Water Filled Steel Boxes as Gap Sealers

Location	Neutron Dose	
	(mrem/shot)	(+/- error)
1	9331	2
2	1.19	0.004
3	0.489	0.0020
4	0.174	0.0048
5	0.023	0.0006
6	0.005	0.0001
7	16.4	0.31
8	1.88	0.005
9	0.337	0.0039
10	0.111	0.0009

Table 5.16 Neutron Doses for Pit Shield with Polyethylene Gap Sealers from a  $10^{13}$  Yield of 14 MeV Neutrons

Location	Neutron Dose	
	(mrem/shot)	(+/- error)
1	9332	2
2	1.20	0.005
3	0.585	0.0037
4	0.280	0.0087
5	0.037	0.0013
6	0.007	0.0001
7	18.7	0.49
8	1.75	0.007
9	0.324	0.0058
10	0.109	0.0013

Table 5.17 Neutron Doses for Pit Shield with Water Filled Steel Boxes as Gap Sealers from a  $10^{13}$  Yield of 14 MeV Neutrons

The dose to tally point 4 was reduced to 0.174 mrem per shot or about 570 shots per year using the polyethylene blocks as gap sealers, as one can see from table 5.16. For comparison, the water filled steel boxes as gap sealers resulted in a dose to tally point 4 of 0.280 mrem per shot or about 350 shots per year as seen in table 5.17. The pit shield is the cheapest option of the shielding designs with minimal construction or additional materials required, but also results in higher dose than the square shield or the labyrinth.

Since neutron dose had been quantified for all shields, the dose to point 4 due to secondary gamma production by neutrons in shielding materials was examined to determine the importance of adding gamma shielding. As mentioned by a study in the literature review, gamma dose was predicted to be small compared to neutron dose. To test this prediction, a tissue phantom was placed at tally point 4 and energy deposition of gammas was tallied using the same problem geometry as illustrated in figure 5.20. The gamma dose is presented in table 5.18 along with the corresponding neutron dose at that point. One can see that dose from secondary gamma production is negligible at less than 10% of neutron dose. However, dose from primary photons produced in the plasma of the DPF device are not quantified in

this work due to lack of experimental data on energy and quantity. Note that the polyethylene was not borated for the results in table 5.18.

	mrem/shot (+/- mrem)	
Gamma Dose	0.025	0.001
Neutron Dose	0.280	0.009

Table 5.18 Doses to Tally Point 4 from Gammas and Neutrons for the Pit Shield Shown in fig. 5.23

## CHAPTER 6

### CONCLUSIONS

A summary of the doses to tally point 4, the location in the trailer where personnel would receive the highest dose, is presented below in table 6.1. Also presented is the number of times the device could be fired per year while point 4 remains below 100 mrem, the limit set by Bechtel Nevada.

Shield Type	Dose to Tally Point 4 (mrem)	Shots per 100 mrem
<b>Square Shield</b>	0.138	723
<i>with poly outer</i>	0.085	1175
<i>with inner shield</i>	0.055	1821
<b>36in Labyrinth</b>	0.053	1887
<i>non-borated</i>	0.051	1957
<b>18in Labyrinth</b>	0.406	246
<b>Cave Shield</b>	0.446	224
<i>no roof</i>	2.63	38
<b>Pit Shield</b>	0.581	172
<i>poly gap sealer</i>	0.174	574
<i>steel box gap sealer</i>	0.280	357

Table 6.1 Summary of Dose to Tally Point 4 from all Shield Configurations

Ultimately, a decision on which shielding configuration to use will be based on a comparison of the installation and materials costs compared to the number of times the device can be fired. The 36in labyrinth shield would allow the greatest number of shots,

almost 2000 per year, but would also be the most expensive due to the material and installation costs. The pit shield with steel box gap sealers is the most likely preliminary option, as it requires the least amount of materials and installation. Future funding, after demonstration of the device as a versatile D-T neutron source for experimental use, would go towards the construction of a labyrinth shield to increase the number of times the device can be operated. In reality, measured neutron dose will be lower than those predicted in this work due to the built in safety factor of over 2 that was introduced by the use of flux-to-dose conversion factors.

Further studies should include a simulation of the D-D produced 2.45 MeV neutron doses for these shielding configurations. These doses will be significantly lower due to the  $10^{11}$  yield of the D-D reaction, which is 100 times less than the  $10^{13}$  yield of the D-T reaction considered in this study. Additionally, experimental measurements of neutron dose at multiple points should take place after shielding has been installed to verify these MCNPX predictions. An important reason to take dose measurements is locating any unexpected hot spots where radiation is escaping through a gap in the shielding. Finally, a measurement of the X-ray spectrum and intensity emitted by the plasma is necessary. Secondary gammas produced by neutrons in shielding materials were shown to be only 10% of the neutron dose, however a large production of primary X-rays in the DPF device could approach or even exceed the neutron dose. A measurement of primary X-ray energy and quantity would allow MCNPX modeling to determine if gamma shielding is necessary.

## APPENDIX I

### SAMPLE MCNPX INPUT DECK

The following appendix contains a sample input “deck” used in MCNPX. The deck consists of “cards” describing geometries, materials, physics options, tallies, etc. Both the deck and card terms are throwbacks to the days when computers were fed information on punch cards. The input deck describes everything about the problem setup, how MCNPX should run the simulation and what the user wants to tally or calculate. This sample input deck is the actual problem that was run for this project for the final pit shield:

```
Bechtel DPFDRelocation - Pit Shield 11-102
c Updated: 5-10-06
c Author: Robert O'Brien
c
c New Pit Case 3 - Water Filled Steel Tubes
c
c 14 MeV DT neutron source inside 11-102 building
c Concrete Pit Shield
c No capacitor Bank
c No Electron Tallies
c
c |----- CELL CARDS -----|
c
c Pit Walls
10 100 -2.30 -10 11 imp:n,p=1
11 500 -.0012 -11 30 imp:n,p=1
c Concrete Slab Tops
30 100 -2.30 -30 imp:n,p=1
31 100 -2.30 -31 imp:n,p=1
c Poly Tops
40 201 -0.94 -40 imp:n,p=1
41 201 -0.94 -41 imp:n,p=1
c Water Filled Steel Boxes (North-South)
50 300 -7.845 -50 51 imp:n,p=1
51 10 -1.00 -51 imp:n,p=1
52 300 -7.845 -52 53 imp:n,p=1
53 10 -1.00 -53 imp:n,p=1
```

```

c Water Filled Steel Boxes (East-West)
54 300 -7.845 -54 55 imp:n,p=1
55 10 -1.00 -55 imp:n,p=1
56 300 -7.845 -56 57 imp:n,p=1
57 10 -1.00 -57 imp:n,p=1
58 300 -7.845 -58 59 imp:n,p=1
59 10 -1.00 -59 imp:n,p=1
c
c Walls and Ceiling
70 300 -7.845 -70 71 imp:n,p=1
71 500 -.0012 -71 30 31 40 41 50 52 54 56 58 imp:n,p=1
c
c Trailer
81 300 -7.845 -81 82 imp:n,p=1
82 500 -.0012 -82 imp:n,p=1
c
c Dirt
90 400 -1.20 -90 91 10 imp:n,p=1
c Concrete Floor
91 100 -2.30 -91 10 imp:n,p=1
c
c ----- Air -----
99 500 -0.0012 -99 70 81 imp:n,p=1
c
c ----- Universe -----
999 0 99 90 imp:n,p=0

c |----- SURFACE CARDS -----|
c
c Pit Walls
10 BOX 0 0 0 345.44 0 0 0 406.4 0 0 0 -203.2
11 BOX 20.32 20.32 0 304.8 0 0 0 365.76 0 0 0 -182.88
c
c Concrete Slab Lower (8in thick)
30 BOX 20.32 203.2 0 304.8 0 0 0 182.88 0 0 0 -20.32
c Concrete Slab Upper (8in thick)
31 BOX 0 0 30.48 345.44 0 0 0 203.2 0 0 0 20.32
c
c Poly Top North (4in thick)
40 BOX 20.32 233.68 0 304.8 0 0 0 152.4 0 0 0 10.16
c Poly Top South (4in thick)
41 BOX 20.32 0 50.8 304.8 0 0 0 203.2 0 0 0 10.16
c
c Water Filled Steel Box 1 (North-South Western)
50 BOX -10.16 -25.4 0 30.48 0 0 0 457.2 0 0 0 30.48
51 BOX -9.8425 -25.0825 .3175 29.845 0 0 0 456.565 0 0 0 29.845
c Water Filled Steel Box 2 (North-South Eastern)
52 BOX 325.12 -25.4 0 30.48 0 0 0 457.2 0 0 0 30.48
53 BOX 325.4375 -25.0825 .3175 29.845 0 0 0 456.565 0 0 0 29.845
c Water Filled Steel Box 3 (East-West Northern)
54 BOX 20.32 386.08 0 304.8 0 0 0 30.48 0 0 0 30.48
55 BOX 20.6375 386.3975 .3175 304.165 0 0 0 29.845 0 0 0 29.845
c Water Filled Steel Box 4 (East-West Bottom Middle)
56 BOX 20.32 203.2 0 304.8 0 0 0 30.48 0 0 0 30.48
57 BOX 20.6375 203.5175 .3175 304.165 0 0 0 29.845 0 0 0 29.845
c Water Filled Steel Box 5 (East-West Top Middle)
58 BOX 20.32 203.2 30.48 304.8 0 0 0 30.48 0 0 0 30.48

```

```

59 BOX 20.6375 203.5175 30.7975      304.165 0 0   0 29.845 0   0 0
29.845
c
c Steel Walls & Ceiling (1/8in thick)
70 RPP -920.01 396.5575 -248.13 889.47  0 584.07
71 RPP -919.6925 396.24 -247.8125 889.1525  0 583.7525
c
c Trailer 1/8in steel (50x10x10) 21ft from building, 3ft above ground
81 BOX 0 1529.55 91.62 304.8 0 0  0 1524 0  0 0 304.8
82 BOX 0.3175 1529.8675 91.9375 304.165 0 0  0 1523.365 0  0 0 304.165
c
c Dirt
90 RPP -925.01 2470.53 -2446.24 4600 -325.72 0
c Concrete Floor
91 RPP -920.01 396.5575 -248.13 889.47 -15.24 0
c
c ----- Air -----
99 RPP -925.01 2470.53 -2446.24 4600 0 762
c
c Tally location Checks
c 101 SPH 142.48 203.56 -91.62 10
c 102 SPH -549.72 -91.62 122.16 10
c 103 SPH -549.72 794.04 122.16 10
c 104 SPH 173.02 1230.41 213.78 10
c 105 SPH 173.02 2452.01 213.78 10
c 106 SPH 173.02 3979.01 215.78 10
c 107 SPH 173.02 3979.01 215.78 10
c 108 SPH 173.02 3979.01 215.78 10
c 109 SPH 173.02 3979.01 215.78 10
c 110 SPH 173.02 3979.01 215.78 10

c |----- DATA CARDS -----|
c
SDEF ERG=14 par=n pos= 127 279.4 -91.44 $New Source Location
mode p n
nps 1200
prdmp j 1200 1 j 1200
PRINT
c
c phys:p 3j 1
c
c Energy Bins
e0 .001 .01 .1 1 2.5 5 7 10 14
c
c Weight Window Generator
c wwg 105 0
c wwp:n 4j -1
c mesh geom=rec ref=4572 1371.6 121.82  origin=-1 21 1
c      imesh 4573 iints 20
c      jmesh 2742 jints 1
c      kmesh 761 kints 1
c
c Mesh Tally
c tmesh
c rmesh101:n traks
c coral01 -10 99i 6146
c corb101 -10 99i 2793

```

```

c corc101 121.5 122.5
c rmesh201:n traks
c cora201 -10 199i 6146
c corb201 -10 199i 2793
c corc201 121.5 122.5
c endmd
c
c mplot freq 10000 PLOT or 4572 1371 0 ex 2000 pz 121.92 la 0 1 tal201 &
c color on la 0 0
c
c Point Detectors
fq e f
c
fc15 Tally 1 detector
f15:n 142.48 203.56 -91.62 0
c fc115 Tally 11 detector (gamma)
c f115:p 142.48 203.56 -91.62 0
c
fc25 Tally 2 detector
f25:n -549.72 -91.62 122.16 0
c fc125 Tally 12 detector (gamma)
c f125:p -549.72 -91.62 122.16 0
c
fc35 Tally 3 detector
f35:n -549.72 794.04 122.16 0
c fc135 Tally 13 detector (gamma)
c f135:p -549.72 794.04 122.16 0
c
fc45 Tally 4 detector (New Location 6in from trailer wall)
f45:n 152.7175 1545.1075 213.78 0
c fc145 Tally 14 detector (gamma)
c f145:p 173.02 1230.41 213.78 0
c
fc55 Tally 5 detector (New Location 6in from trailer wall)
f55:n 152.7175 3037.9925 213.78 0
c fc155 Tally 15 detector (gamma)
c f155:p 173.02 2452.01 213.78 0
c
fc65 Tally 6 detector (new Location 50ft from trailer end)
f65:n 152.7175 4592.4725 213.78 0
c fc165 Tally 16 detector (gamma)
c f165:p 173.02 3979.01 213.78 0
c
fc75 Tally 7 detector (1in Outside Ceiling)
f75:n 127 279.4 586.61 0
c fc175 Tally 17 detector (gamma)
c f175:p 127 279.4 586.61 0
c
fc85 Tally 8 detector (21ft from building)
f85:n 785.374 -581.551 121.92 0
c fc185 Tally 18 detector (gamma)
c f185:p 954.32 -714.39 121.92 0
c
fc95 Tally 9 detector (52ft from building)
f95:n 1359.342 -1332.124 121.92 0
c fc195 Tally 19 detector (gamma)
c f195:p 1566.89 -1433.8 121.92 0

```

c  
fc105 Tally 10 detector (86ft from building)  
f105:n 1988.854 -2155.333 121.92 0  
c fc205 Tally 20 detector (gamma)  
c f205:p 2258.5 -2246.05 121.92 0  
c  
c PROBLEM MATERIALS  
c  
c (Water density=1.00g/cc)  
m10 8016 -.89 1001 -.11  
c  
c Concrete  
c (Density = 2.30g/cc)  
c (REF: NIST <http://physics.nist.gov/cgi-bin/Star/compos.pl>)  
m100 1001 -.010 6012 -.001 8016 -.529  
11023 -.016 12000 -.002 13027 -.034  
14000 -.337 19000 -.013 20000 -.044  
26000 -.014  
c  
c 5% Borated Poly  
c (Density = 0.95g/cc)  
c (REF: <http://www.thermo.com/com/cda/product/detail/1,1055,22378,00.html>)  
c m200 1001 -.136525 6012 -.813475 5010 -.0099 5011 -.0401  
c  
c Non-Borated Poly  
c (Density = 0.94g/cc)  
c (REF:NIST [physics.nist.gov/cgi-bin/Star/compos.pl?matno=221](http://physics.nist.gov/cgi-bin/Star/compos.pl?matno=221))  
m201 1001 -.143711 6012 -.856289  
c  
c Paraffin Wax  
c (Density = 0.93g/cc)  
c (REF=NIST)  
c m202 1001 -.148605 6012 -.851395  
c  
c Wall Material (STEEL AISI 1040)  
c (Steel Density=7.845g/cc)  
c (REF: <http://www.efunda.com>)  
c (Composition: 98.94wt% Fe, 0.37wt% C, 0.6wt% Mn, 0.04wt% P, 0.05wt% S)  
m300 26000 -.9894 6012 -.0037 25055 -.0060 15031 -.0004 16000 -.0005  
c  
c Dirt  
c Nevada Type 2 (DNA E-M-1)  
m400 11023 -.0130 13027 -.0670 26056 -.0220 14028 -.3224 22000 -.0027  
20040 -.0240 19000 -.0270 1001 -.0070 16032 -.0003 12000 -.0060  
15031 -.0004 8016 -.5082  
c  
c Air  
c (Dry, Sea Level Density=0.0012g/cc)  
c (REF: NIST)  
c (Composition: 75.5267wt% N, 23.1781wt% O, 1.2827wt% Ar, .0125wt% C)  
m500 7014 -.755267 8016 -.231781 18000 -.012827 6012 -0.000125  
c  
c Capacitor Fill (Polyethylene)  
c (Density=0.94g/cc)  
c (REF: NIST)  
c m600 6012 -.8563 1001 -.1437

## APPENDIX II

### SAMPLE MCNPX OUTPUT DECK

An output deck is the text output produced by MCNPX after running a problem. MCNPX can also produce data files for plotting tally data. The text output deck prints all information about the simulation including results, statistical results and how particles were transported during the run. The attached output deck is greatly edited down to only key tables, as the full output deck would constitute over 200 pages. This run would have taken 5731 minutes or 95 hours on a single computer. Using the UNLV Beowulf cluster, this runtime was reduced to less than an hour.

```
lmcnpX    version 26a   ld=Mon Dec 05 08:00:00 MST 2005
05/11/06 03:05:36
```

```
*****
*****      probid =    05/11/06 03:05:36
n=14pit-20060510
```

```
*****
*
*          Copyright Notice for MCNPX          *
*
* This program was prepared by the Regents of the *
* University of California at Los Alamos National *
* Laboratory (the University) under contract number *
* W-7405-ENG-36 with the U.S. Department of Energy *
* (DOE). The University has certain rights in the *
* program pursuant to the contract and the program *
* should not be copied or distributed outside your *
* organization. All rights in the program are *
* reserved by the DOE and the University. Neither *
* the U.S. Government nor the University makes any *
* warranty, express or implied, or assumes any *
* liability or responsibility for the use of this *
* software. *
*
```

\*\*\*\*\*

1tally 15  
print table 30

+ Tally 1 detector  
tally type 5 particle flux at a point detector.  
particle(s): neutron

order of printing: e f

point detector specifications

detector	x	y	z	r0
1	1.42480E+02	2.03560E+02	-9.16200E+01	0.00000E+00

energy bins

0.00000E+00	to	1.00000E-03	mev
1.00000E-03	to	1.00000E-02	mev
1.00000E-02	to	1.00000E-01	mev
1.00000E-01	to	1.00000E+00	mev
1.00000E+00	to	2.50000E+00	mev
2.50000E+00	to	5.00000E+00	mev
5.00000E+00	to	7.00000E+00	mev
7.00000E+00	to	1.00000E+01	mev
1.00000E+01	to	1.40000E+01	mev

1material composition

print table 40

material

number	component nuclide, atom fraction			
10	8016, 3.37660979703E-01	1001, 6.62339020297E-01		
100	1001, 1.68755658580E-01	6012, 1.41730146392E-03		
8016, 5.62493139093E-01	11023, 1.18366510591E-02			
	12000, 1.39951296937E-03	13027, 2.14316541058E-02		
14000, 2.04075605118E-01	19000, 5.65495230121E-03			
	20000, 1.86719584151E-02	26000, 4.26356689460E-03		
201	1001, 6.66480263824E-01	6012, 3.33519736176E-01		
300	26000, 9.75440707308E-01	6012, 1.69764892878E-02		
25055, 6.01319684046E-03	15031, 7.11039043653E-04			
	16000, 8.58567520338E-04			
400	11023, 1.02253529179E-02	13027, 4.49032389603E-02		
26056, 7.11228355599E-03	14028, 2.08384113065E-01			
	22000, 1.01974944431E-03	20040, 1.08599337815E-02		
19000, 1.24874985128E-02	1001, 1.25597928264E-01			
	16032, 1.69675862546E-04	12000, 4.46400090295E-03		
15031, 2.33526202146E-04	8016, 5.74542698531E-01			
500	7014, 7.84426823501E-01	8016, 2.10751763655E-01		
18000, 4.66991582820E-03	6012, 1.51497015244E-04			

1particles and energy limits

print table 101

always	always	particle	maximum	smallest	largest
--------	--------	----------	---------	----------	---------

use table	use model	cutoff	particle	table	table
particle type		energy	energy	maximum	maximum
below	above				
1 n neutron		0.0000E+00	1.0000E+37	2.0000E+01	
1.5000E+02	2.0000E+01	1.5000E+02			
2 p photon		1.0000E-03	1.0000E+02	1.0000E+05	
1.0000E+05	1.0000E+37	1.0000E+37			
3 e electron		1.0000E-03	1.0000E+02	1.0000E+02	
1.0000E+02	1.0000E+37	1.0000E+37			

lproblem summary

run terminated when 25000000 particle histories were done.

+

05/11/06 07:39:02

Bechtel DPDFD Relocation - Pit Shield 11-102

probid = 05/11/06 03:05:36

neutron creation	tracks	weight	energy	neutron
loss	tracks	weight	energy	
(per source particle)				
source	25000000	1.0000E+00	1.4000E+01	escape
2347895	5.6090E-02	2.8625E-01		
nucl. interaction	0	0.	0.	energy
cutoff	0	0.	0.	
particle decay	0	0.	0.	time
cutoff	0	0.	0.	
weight window	0	0.	0.	weight
window	0	0.	0.	
cell importance	0	0.	0.	cell
importance	0	0.	0.	
weight cutoff	0	2.0964E-01	4.3969E-02	weight
cutoff	23050922	2.0970E-01	4.3895E-02	
energy importance	0	0.	0.	energy
importance	0	0.	0.	
dxtran	0	0.	0.	dxtran
0	0.	0.	0.	
forced collisions	0	0.	0.	forced
collisions	0	0.	0.	
exp. transform	0	0.	0.	exp.
transform	0	0.	0.	
upscattering	0	0.	3.8755E-07	
downscattering	0	0.	9.2348E+00	
photonuclear	0	0.	0.	capture
48723	9.5651E-01	4.3619E+00		
(n, xn)	895080	2.5307E-02	5.6697E-02	loss to
(n, xn)	447540	1.2654E-02	1.7392E-01	
prompt fission	0	0.	0.	loss to
fission	0	0.	0.	
delayed fission	0	0.	0.	nucl.
interaction	0	0.	0.	particle
decay	0	0.	0.	

tabular boundary	0	0.	0.	tabular
boundary	0	0.	0.	
tabular sampling	0	0.	0.	
total	25895080	1.2349E+00	1.4101E+01	total
25895080	1.2349E+00	1.4101E+01		
number of neutrons banked			447540	average time
of (shakes)				
neutron tracks per source particle			1.0358E+00	escape
1.6001E+05	tco	1.0000E+34		
neutron collisions per source particle			1.2655E+02	capture
6.3798E+04	eco	0.0000E+00		
total neutron collisions			3163774070	capture or
escape 6.9128E+04	wc1	-5.0000E-01		
net multiplication			1.0127E+00 0.0000	any
termination 8.2976E+04	wc2	-2.5000E-01		
photon creation	tracks	weight	energy	photon
loss	tracks	weight	energy	
			(per source particle)	
(per source particle)				
source	0	0.	0.	escape
3545973	1.4359E-01	2.8020E-01		
nucl. interaction	0	0.	0.	energy
cutoff	0	0.	2.7375E-04	
particle decay	0	0.	0.	time
cutoff	0	0.	0.	
weight window	0	0.	0.	weight
window	0	0.	0.	
cell importance	0	0.	0.	cell
importance	0	0.	0.	
weight cutoff	0	0.	0.	weight
cutoff	0	0.	0.	
energy importance	0	0.	0.	energy
importance	0	0.	0.	
dxtran	0	0.	0.	dxtran
0	0.	0.		
forced collisions	0	0.	0.	forced
collisions	0	0.	0.	
exp. transform	0	0.	0.	exp.
transform	0	0.	0.	
from neutrons	62611207	2.5487E+00	8.0514E+00	compton
scatter	0	0.	6.7708E+00	
bremsstrahlung	32903300	1.3352E+00	1.3979E-01	capture
106746778	4.3405E+00	2.4071E-01		
p-annihilation	9987370	4.0488E-01	2.0690E-01	pair
production	4993685	2.0244E-01	1.1079E+00	
photonuclear	0	0.	0.	
photonuclear abs	0	0.	0.	
electron x-rays	0	0.	0.	
1st fluorescence	9784559	3.9779E-01	1.8109E-03	
2nd fluorescence	0	0.	0.	
(gamma, xgamma)	0	0.	0.	
tabular sampling	0	0.	0.	
total	115286436	4.6865E+00	8.3999E+00	total
115286436	4.6865E+00	8.3999E+00		

number of photons banked	100508192	average time
of (shakes)	cutoffs	
photon tracks per source particle	4.6115E+00	escape
5.1977E+04	tco 1.0000E+34	
photon collisions per source particle	2.8919E+01	capture
3.9295E+04	eco 1.0000E-03	
total photon collisions	722962822	capture or
escape 3.9701E+04	wc1 -5.0000E-01	any
termination 3.7986E+04	wc2 -2.5000E-01	
computer time so far in this run	5731.33 minutes	maximum
number ever in bank	19	
computer time in mcrun	5731.15 minutes	bank
overflows to backup file	0	
source particles per minute	4.3621E+03	dynamic
storage 0 words,	0 bytes.	
random numbers generated	62632242093	most random
numbers used was 32693 in history	11693945	
total 62611207	1.00000E+00	2.54866E+00
1.00000E+00		
ltally 15	nps = 25000000	
+	Tally 1 detector	
tally type 5	particle flux at a point detector.	
units 1/cm**2		
particle(s): neutron		

detector:	1	
energy		
1.0000E-03	5.23439E-06	0.0005
1.0000E-02	4.23741E-07	0.0014
1.0000E-01	5.44072E-07	0.0024
1.0000E+00	1.23077E-06	0.0007
2.5000E+00	9.38335E-07	0.0007
5.0000E+00	7.04432E-07	0.0008
7.0000E+00	2.50365E-07	0.0012
1.0000E+01	9.82541E-08	0.0020
1.4000E+01	1.36193E-05	0.0002
total	2.30437E-05	0.0002

uncollided neutron flux

detector:	1	
energy		
1.0000E-03	0.00000E+00	0.0000
1.0000E-02	0.00000E+00	0.0000
1.0000E-01	0.00000E+00	0.0000
1.0000E+00	0.00000E+00	0.0000
2.5000E+00	0.00000E+00	0.0000
5.0000E+00	0.00000E+00	0.0000
7.0000E+00	0.00000E+00	0.0000
1.0000E+01	0.00000E+00	0.0000
1.4000E+01	1.32017E-05	0.0000
total	1.32017E-05	0.0000

detector located at x,y,z = 1.42480E+02 2.03560E+02-9.16200E+01

detector score diagnostics		cumulative	tally
cumulative		fraction of	per
fraction of	transmissions	transmissions	history
times average score			
total tally			
1.00000E-01	0	0.00000	0.00000E+00
0.00000			
1.00000E+00	0	0.00000	0.00000E+00
0.00000			
2.00000E+00	0	0.00000	0.00000E+00
0.00000			
5.00000E+00	0	0.00000	0.00000E+00
0.00000			
1.00000E+01	0	0.00000	0.00000E+00
0.00000			
1.00000E+02	0	0.00000	0.00000E+00
0.00000			
1.00000E+03	0	0.00000	0.00000E+00
0.00000			
1.00000E+38	0	0.00000	0.00000E+00
0.00000			
before dd roulette	2422703816	1.00000	2.30437E-05
1.00000			

average tally per history = 2.30437E-05      largest score =  
 3.34545E-02  
 (largest score)/(average tally) = 1.45179E+03      nps of largest score =  
 12062649

score contributions by cell						
	cell	misses	hits	tally per history	weight per hit	
1	10	2732073801	112561097	6.44510E-06	1.44826E-07	
2	11	11391	28002221	1.37244E-05	1.22529E-05	
3	30	58666523	238856910	2.23068E-06	2.33475E-07	
4	31	25484542	99175403	5.65564E-07	1.42567E-07	
5	40	91487519	130962841	8.94143E-10	1.70686E-10	
6	41	24222769	38693485	8.23252E-11	5.31906E-11	
7	50	23879	1070348	1.25938E-08	2.94152E-07	
8	51	20661444	25692714	2.09564E-08	2.03914E-08	
9	52	19944	811672	7.61146E-09	2.34438E-07	
10	53	14801267	20299113	1.50913E-08	1.85862E-08	
11	54	31580	437044	3.41773E-13	1.95502E-11	
12	55	11489594	6856246	7.08304E-13	2.58270E-12	
13	56	61844	1492856	1.42235E-10	2.38192E-09	
14	57	28364779	32554312	3.75341E-10	2.88242E-10	
15	58	118819	186808	1.33706E-13	1.78935E-11	
16	59	10308138	797920	5.37936E-13	1.68543E-11	
17	70	171352	850410	1.42405E-10	4.18637E-09	
18	71	92027	587667	1.00687E-08	4.28336E-07	
19	81	8169	5707	2.41782E-18	1.05915E-14	
20	82	1134	457	5.44779E-20	2.98019E-15	
21	90	171071974	649278252	9.78665E-09	3.76828E-10	
22	91	12493076	33119439	2.14508E-10	1.61920E-10	
23	99	171465	410894	2.07533E-11	1.26269E-09	
	total	7429706092	2422703816	2.30437E-05	2.37789E-07	

```

score misses
  russian roulette on pd          0
  psc=0.                          622760030
  russian roulette in transmission 0
  underflow in transmission      120210579
  hit a zero-importance cell      0
  energy cutoff                   0

```

1analysis of the results in the tally fluctuation chart bin (tfc) for  
tally 15 with nps = 25000000 print table 160

```

normed average tally per history = 2.30437E-05      unnormed average
tally per history = 2.30437E-05                    estimated
estimated tally relative error = 0.0002            relative error
variance of the variance = 0.0207
relative error from zero tallies = 0.0000
from nonzero scores = 0.0002

number of nonzero history tallies = 25000000      efficiency for
the nonzero tallies = 1.0000                      largest
history number of largest tally = 12062649
unnormalized history tally = 3.34828E-02          (largest
(largest tally)/(average tally) = 1.45301E+03    tally)/(avg nonzero tally)= 1.45301E+03

(confidence interval shift)/mean = 0.0000        shifted
confidence interval center = 2.30439E-05

```

if the largest history score sampled so far were to occur on the next history, the tfc bin quantities would change as follows:

estimated quantities value(nps+1)/value(nps)-1.	value at nps	value at nps+1
mean	2.30437E-05	2.30450E-05
0.000058		
relative error	1.96838E-04	2.05216E-04
0.042563		
variance of the variance	2.07178E-02	2.39467E-02
0.155853		
shifted center	2.30439E-05	2.30439E-05
0.000002		
figure of merit	4.50339E+03	4.14319E+03
-0.079985		

the estimated inverse power slope of the 200 largest tallies starting at 1.35047E-03 is 2.4439  
the history score probability density function appears to have an unsampled region at the largest history scores: please examine.

\*\*\*\*\* the nps-dependent tfc bin check results are suspect because there are only 1 nps tally values to analyze \*\*\*\*\*

```
=====
=====
```

results of 10 statistical checks for the estimated answer for  
the tally fluctuation chart (tfc) bin of tally 15

tfc bin	--mean--	-----relative error-----	-----		
variance of the variance	behavior	value	--figure of merit--	-pdf-	value
decrease	decrease rate	value	decrease behavior	decrease rate slope	
desired	random	<0.05	yes	1/sqrt(nps)	<0.10
yes	1/nps	constant	random	>3.00	
observed	random	0.00	yes	yes	0.02
yes	yes	constant	random	2.44	
passed?	yes	yes	yes	yes	yes
yes	yes	yes	yes	no	

```
=====
=====
```

run terminated when 25000000 particle histories were done.

computer time = 5731.33 minutes

mcpnx version 26a Mon Dec 05 08:00:00 MST 2005  
05/11/06 07:39:02 probid = 05/11/06 03:05:36

## BIBLIOGRAPHY

- Attix, F., Introduction to Radiological Physics and Radiation Dosimetry, John Wiley and Sons. 1986.
- Cember, H., Introduction to Health Physics, McGraw-Hill. 1996.
- El-Wakil, M., Nuclear Power Engineering, McGraw-Hill. 1962.
- Freeman, B. L. et al., "Neutron Emission Characteristics of a High-Current Plasma Focus: Initial Studies."
- Frignani, M. et al., "Monte Carlo simulation of neutron backscattering from concrete walls in the dense plasma focus laboratory of Bologna University." 2005.
- Kim, J. et al., "Design of Radiation Shielding for the Proton Therapy Facility at the National Cancer Center in Korea." 2005.
- Krane, K., Introductory Nuclear Physics, John Wiley and Sons. 1988.
- Lamarsh, J.R., Introduction to Nuclear Engineering, 2<sup>nd</sup> edition. New York: Addison-Wesley. 1983.
- NCRP Report No. 38, Protection Against Neutron Radiation. 1971.
- O'Brien, R., "Shielding and Radiation Dose Analysis of a Dense-Plasma Focus Device," ANS RPSD Poster Session. 2006.
- Pelowitz, D.B., MCNPX<sup>TM</sup> User's Manual, Version 2.5.0. April 2005.
- Raspa, V. et al., "Determination of the Effective Energy of Pulsed Powerful Hard X-Ray Sources based on Pinch Plasma Focus Discharges."
- Shleien, B., The Health Physics and Radiological Health Handbook, Scinta, Inc. 1992.
- Tesch, K., "A Simple Estimation of the Lateral Shielding for Proton Accelerators in the Energy Range 50 to 1000 MeV." 1985.

Titt, U., Newhauser, W. D., "Neutron Shielding Calculations in a Proton Therapy Facility Based on Monte Carlo Simulations and Analytical Models: Criterion for Selecting the Method of Choice." 2005.

Torres et al., "Comparison of MCNP5 and Experimental Results on Neutron Shielding Effects for Materials." 2004.

Turner, J., Atoms, Radiation and Radiation Protection, John Wiley and Sons. 1995.

U.S. Nuclear Regulatory Commission Regulations 10CFR20.

## VITA

Graduate College  
University of Nevada, Las Vegas

Robert James O'Brien

### Local Address:

4505 Maryland Parkway  
Las Vegas, Nevada 89154-4027

### Home Address:

840 Viento Del Montagna  
Henderson, Nevada 89012

### Degrees:

Bachelor of Science, Applied Physics, 2005  
University of Nevada, Las Vegas

Bachelor of Science, Mechanical Engineering, 2005  
University of Nevada, Las Vegas

### Professional Memberships and Societies:

American Nuclear Society (ANS)  
American Physical Society (APS)  
American Society of Mechanical Engineers (ASME)  
National Society of Professional Engineers (NSPE)  
Society of Physics Students  
Tau Beta Pi Engineering Honors Society

### Special Honors and Awards:

National Science Foundation Research Experience for Undergraduates, 2003  
NASA Undergraduate Space Grant, 2002-2004  
Harold and Mayme Stocker Scholarship, 2001-2005  
Outstanding Mechanical Engineering Student of the Year, 2004  
Outstanding Graduate, Mechanical Engineering, 2005  
Dean's List 8 Semesters as Undergraduate  
Honor's College, UNLV 2000-2005

**Publications:**

American Nuclear Society Student Conference 2004, Presentation  
“Criticality and Heat Transfer Analysis of a Np/Pu Mixture”

ANS Radiation Protection and Shielding Division Topical Conference 2006, Poster  
“Shielding and Radiation Dose Analysis of a Dense-Plasma Focus Device”

ANS Annual Winter Conference 2006, Paper (Upcoming)  
“Shielding and Radiation Dose Analysis for a Dense-Plasma Focus Neutron Source”

Thesis Title: Shielding and Radiation Dose Analysis for a Dense-Plasma Focus Neutron  
Source

**Thesis Examination Committee:**

Chairperson, Dr. William Culbreth, Ph.D.

Committee Member, Dr. Chen, Ph.D.

Committee Member, Dr. Roy, Ph.D.

Graduate Faculty Representative, Dr. Shields, Ph.D.